Accepted Manuscript

4*β*-amidotriazole linked podophyllotoxin congeners: DNA topoisomerase-IIα inhibition and potential anticancer agents for prostate cancer

V. Ganga Reddy, Srinivasa Reddy Bonam, T. Srinivasa Reddy, Ravikumar Akunuri, V.G.M. Naidu, V. Lakshma Nayak, Suresh K. Bhargava, H.M.Sampath Kumar, P. Srihari, Ahmed Kamal

PII: S0223-5234(17)31082-6

DOI: 10.1016/j.ejmech.2017.12.050

Reference: EJMECH 10028

To appear in: *European Journal of Medicinal Chemistry*

Received Date: 20 October 2017

Revised Date: 12 December 2017

Accepted Date: 13 December 2017

Please cite this article as: V.G. Reddy, S.R. Bonam, T.S. Reddy, R. Akunuri, V.G.M. Naidu, V.L. Nayak, S.K. Bhargava, H.M.S. Kumar, P. Srihari, A. Kamal, 4*β*-amidotriazole linked podophyllotoxin congeners: DNA topoisomerase-IIα inhibition and potential anticancer agents for prostate cancer, *European Journal of Medicinal Chemistry* (2018), doi: 10.1016/j.ejmech.2017.12.050.

Graphical Abstract

4*β*-Amidotriazole linked podophyllotoxin congeners: DNA topoisomerase-IIα inhibition and potential anticancer agents for prostate cancer

V. Ganga Reddy, Srinivasa Reddy Bonam, T. Srinivasa Reddy,* Ravikumar Akunuri, V. G. M. Naidu, V. Lakshma Nayak, Suresh K. Bhargava, H. M. Sampath Kumar, P. Srihari,* Ahmed Kamal*

Graphical Abstract:

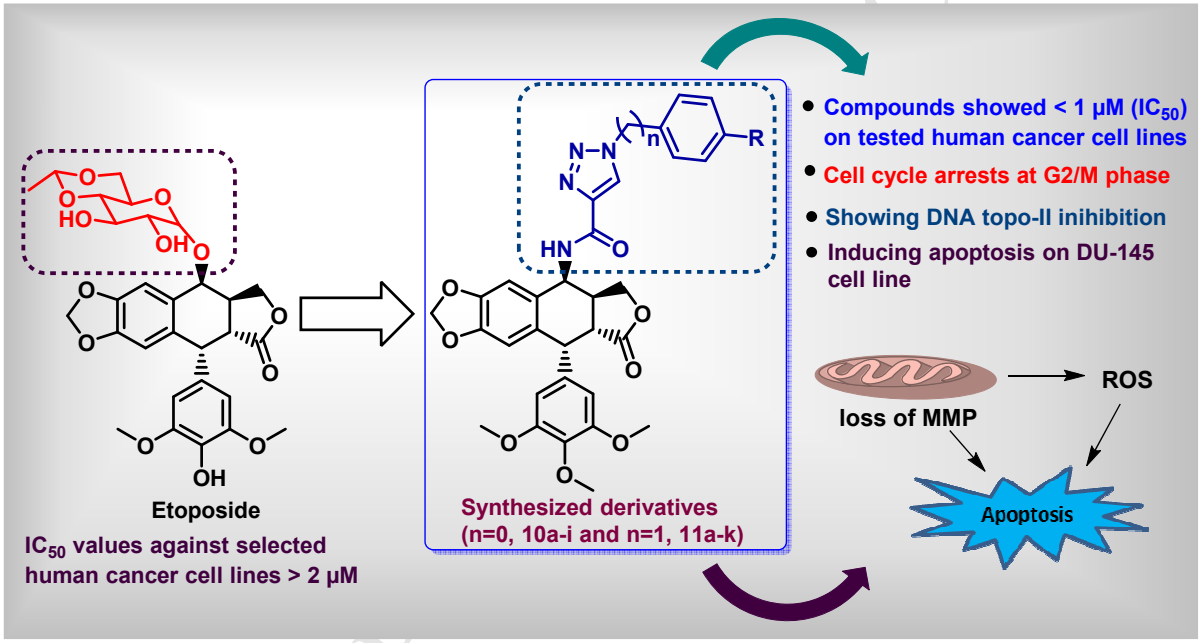

4β-Amidotriazole linked podophyllotoxin congeners: DNA topoisomerase-IIα inhibition and potential anticancer agents for prostate cancer

V. Ganga Reddy,[a, b, c] Srinivasa Reddy Bonam,[a, d] T. Srinivasa Reddy,*[g] Ravikumar Akunuri,[e] V. G. M. Naidu,[e] V. Lakshma Nayak,[b] Suresh K. Bhargava,[g] H. M. Sampath Kumar,[a, d] P. Srihari,*[a, c] Ahmed Kamal*[a, b, e, f]

[a]*Academy of Scientific and Innovative Research (AcSIR), CSIR-Indian Institute of Chemical Technology (IICT), Hyderabad, 500007, India*

[b]*Medicinal Chemistry and Biotechnology, CSIR-Indian Institute of Chemical Technology (IICT), Hyderabad 500007, India*

[c]*Division of Natural Products Chemistry, CSIR-Indian Institute of Chemical Technology (IICT), Hyderabad 500007, India*

[d]*Vaccine Immunology Laboratory, Natural Products Chemistry Division, CSIR-Indian Institute of Chemical Technology (IICT), Hyderabad, 500007, India*

[e]*Department of Medicinal Chemistry, National Institute of Pharmaceutical Education and Research (NIPER), Hyderabad, 500037, India*

[f]*School of Pharmaceutical Education and Research, Jamia Hamdard University, New Delhi, 110062, India*

[g]*Centre for Advanced Materials & Industrial Chemistry (CAMIC), School of Science, RMIT University, GPO BOX 2476, Melbourne 3001, Australia*

***Corresponding authors:** E-mail addresses: ahmedkamal@iict.res.in (Dr. Ahmed Kamal), srihari@iict.res.in (Dr. P. Srihari), srinivasareddy.telukutla@rmit.edu.au (Dr. Srinivasa Reddy Telukutla)

Abstract: Topoisomerases (topo-I and topo-II) have occupied a significant role in DNA replication, transcription, and are a promising set of antitumor targets. In the present approach, a series of new 4β-amidotriazole linked podophyllotoxin derivatives (**10a-i** and **11a-k**) were designed, synthesized by employing the click chemistry and their biological activities were evaluated. The majority of derivatives showed promising antiproliferative activity with IC_{50} values ranging from 1-10 μM on the six human cancer cell lines; cervical (HeLa), breast (MCF-7), prostate (DU-145), lung (A549), liver (HepG2) and colon (HT-29). Among them, some of the congeners **10b**, **10g** and **10i** have shown remarkable cytotoxicity with IC_{50} values of, < 1 μM against the tested cancer cell lines and found to be more active than etoposide. Topoisomerase-mediated DNA relaxation assay results showed that the derivatives could efficiently inhibit the activity of topoisomerase-II. In addition, flow cytometry analysis on DU-145 cells revealed that these compounds arrest G2/M phase of cell cycle. Further apoptotic studies were also performed on these DU-145 cells, which showed that this class of compounds could induce apoptosis effectively.

Keywords: Triazole; topo-II inhibition; anticancer activity; cell cycle; apoptosis

Introduction

Chemotherapy is one of the most prominent treatment approaches for cancer [1]. Even though a huge number of anticancer drugs are available in the market, their utility is limited due to prominent side effects instead of their selective toxicity and outcome of resistance [2]. The ultimate goal of cancer chemotherapy is to produce a drug that can selectively destroy cancer cells without having any significant effects on normal cells. Moreover, intense efforts have focused on the development of novel antitumor agents with selective cytotoxicity against resistance tumor cells.

Natural products have long served as lead compounds for the development of molecules with optimized pharmacological properties for a variety of diseases, including cancer [3-5]. In this context, podophyllotoxin is a well-established lead in the development of new chemical agents for the treatment of cancer [6]. The semi-synthetic derivatives of podophyllotoxin like etoposide and teniposide inhibit DNA topoisomerase-II by stabilizing the topoisomerase-II via binding covalently with DNA and are used against a variety of cancers [7-8]. However, their therapeutic use has encountered certain limitations such as acquired drug resistance [9], cytotoxicity towards normal cells, poor aqueous solubility [10]. Extensive synthetic efforts have been carried out by a number of research groups to improve the selectivity as well as

DNA topoisomerase-II inhibition [11-13]. Previous reports suggested that the core structural features like transfused γ-lactone, fused dioxole ring, and the orthogonal free-rotating 3,4,5-trimethoxyphenyl fragment are considered essential for the cytotoxic activity of podophyllotoxin derivatives [14-15]. It has also been indicated in the literature that bulkier substituents at C-4 position of podophyllotoxin usually enhances the cytotoxicity and DNA topoisomerase-II inhibition activity [16-17]. Currently, some of these synthetic podophyllotoxin derivatives are being used in the treatment of several cancers [18-19] and many of them have entered clinical trials for the treatment of diverse neoplasms (**Figure 1**). It was found that most of these podophyllotoxin derivatives induce apoptosis by inhibiting topoisomerase II [20]. Hence, a significant piece of attention has been diverted towards the structural modification of podophyllotoxin to develop new therapeutic agents because of the development of resistance towards etoposide [21-23].

On the other aspect, nitrogen containing heterocyclic motifs such as triazoles play a key role in enhancing the cytotoxicity towards the cancer cells because of their improved solubility and pharmacokinetic parameters at the binding site [24-25]. In addition, 1,2,3-triazoles have a high dipole moment and are able to participate actively in hydrogen bonding as well as in dipole-dipole and π stacking interactions, which help them in binding easily with the biological targets to improve their solubility [26]. In continuation of our efforts to improve the cytotoxicity of podophyllotoxin [27], herein we report the design and synthesis of a series of 4*β*-amidotriazole linked podophyllotoxin derivatives to improve its potency by the incorporation of the amido-triazolic group at the C-4 position, which can increase the solubility and pharmacokinetic parameters of the podophyllotoxin skeleton.

< **Fig. 1** >

2. Results and Discussion

2.1. Chemistry

The synthetic route adopted to obtain compounds (**10a-i** and **11a-k**) is depicted in **Scheme 1**. The main precursor's aryl azides (**1a-i**), benzyl azides (**2a-k**) and 4*β*-aminopodophyllotoxin (**9**) were prepared by using reported methods [28]. The triazole acid intermediates (**6a-i** and **7a-k**) were synthesized by the reaction of ethyl propiolate with different azides by employing the click chemistry protocol to produce triazolic esters (**4a-i** and **5a-k**), which upon base hydrolysis afforded triazolic acids (**6a-i** and **7a-k**) in good yields. Subsequently, the acids

were coupled with 4*β*-aminopodophyllotoxin (**9**) in the presence of *N*-(3-dimethylaminopropyl)-*N′*-ethylcarbodiimide hydrochloride (EDCI), and 1-hydroxybenzotriazole (HOBT) in anhydrous DMF under nitrogen atmosphere to provided the desired 4*β*-amidotriazole linked podophyllotoxin derivatives (**10a-i** and **11a-k**) in best yields (75-90%) and all these compounds were characterized by spectroscopic studies (NMR, MS, and HRMS).

< **Scheme 1** >

< **Scheme 2** >

2.2. Antiproliferative activity

MTT assay [29] was performed to evaluate the cytotoxic effects of all newly synthesized analogues of 4*β*-amidotriazole linked podophyllotoxin against the selected human cancer cell lines, and the results were summarized as IC_{50} values in **Table 1**. As shown in **Table 1**, several of the 4*β*-amidotriazole linked podophyllotoxin derivatives showed enhanced *in vitro* cytotoxic activity with IC_{50} values of 1-10 μM, whereas the compounds did not show significant cytotoxicity on NIH/3T3 skin fibroblast cells and some of the compounds **10a**, **10b**, **10g**, **10i**, **11b** and **11h** displayed potent broad-spectrum of activities against all the tested cell lines. The compounds **10b**, **10g,** and **10i** exhibited significant cytotoxicity with the IC_{50} values of < 1 μM and were superior to etoposide. Moreover, compound **10g** exhibited remarkable cytotoxicity with the IC_{50} values in the range of 0.70-4.11 μM and was most promising compound in the series. For instance, cervical (Hela), breast (MCF-7), prostate (DU-145), lung (A549), liver (HepG2) and colon (HT-29) were affected by **10g** with IC_{50} values of 0.78, 0.97, 0.70, 1.20, 0.78 and 4.11 μM, respectively. Likewise, **10b** exhibited 6.49, 1.10, 0.99, 1.61, 2.79 and 11.4 μM whereas **10i** showed 1.21, 1.35, 0.89, 1.96, 1.21 and 4.40 μM against these human cancer cell lines (HeLa, MCF-7, DU-145, A549, HepG2 and HT-29), respectively and the IC_{50} of etoposide employed as a standard drug ranges from 1.62 to 2.84 μM.

Based on the cytotoxicity results, the structure-activity relationship (SAR) was examined for these 4*β*-amidotriazole linked podophyllotoxin derivatives (**10a-i** and **11a-k**) to investigate the effect of electron donating methoxy, methylenedioxy as well as electron withdrawing groups like chloro, fluoro and trifluoromethyl groups on cancer cell toxicity. By comparing the cytotoxicity values of compounds with different substitutions, it was clearly observed that

the aryl triazolic-amide derivatives (**n = 0, 10a-i**) shown higher cytotoxicity in comparison to their corresponding benzyl triazolic-amide derivatives (**n = 1, 11a-k**). In case of aryl triazolic-amide derivatives, chloro substituent containing compound (**10g**) at position-4 exhibited high cytotoxicity (0.70-4.11 µM) against the tested cell lines and trifluoro methyl, methoxy substituted compounds (**10b;** 0.99-11.40 µM and **10i;** 0.89-4.40 µM) have also shown promising inhibition values than the other substituents i.e., fluoro, 3,4-dimethoxy, 3,4,5-trimethoxy and 3,4-methylenedioxy groups baring compounds. Subsequently, the benzyl triazolic-amide derivatives of podophyllotoxin (**11a-k**) displayed moderate cytotoxicity. The cytotoxicity data indicates that the strong electron withdrawing groups like chloro, trifluoromethyl at position-4 in aryl triazolic-amide derivatives exhibited superior cytotoxicity than the standard.

< **Table 1** >

2.3. Cell cycle analysis

To understand the mode of action of the most active compounds (**10b**, **10g,** and **10i**), we examined the effects on cell cycle [30] by flow cytometry in DU-145 cancer cells. In this study, DU-145 cells were treated with mentioned compounds for 24 h at indicated concentrations. The compounds **10b**, **10g,** and **10i** at 0.5 µM showed 56.71%, 31.94% and 52.42% and at 1 µM 64.3%, 35.61% and 56.16% of cell accumulation in G2/M phase, whereas **VP-16** (etoposide) showed 71.53% at 2 µM concentrations (Fig. 2). The data obtained clearly indicated that these compounds including **VP-16** leads to G2/M cell cycle arrest of DU-145 cells.

< **Fig. 2** >

2.4. DNA topoisomerase-II inhibition assay

Topoisomerase II inhibition assay was performed by using Topoisomerase II Drug Screening Kit (TG1009, TopoGEN, USA) with etoposide as the standard. The DNA substrate, pHOT1 was included in the assay as supercoiled DNA, because of its small size and easy to handle and has a large number of Topo II recognition elements. The assay system is based on evaluating the formation of DNA cleavage products, primarily linearized DNA (linear DNA) by topo-II enzymes [31-32].

< **Fig. 3** >

From the results, it was observed that catenated DNA treated with topoisomerase II (5units) has shown nicked circular and relaxed circular DNA without any catenated DNA in the wells as represented in the lane D (Fig. 3). Catenated DNA in the presence of topoisomerase II incubated with etoposide (Lane E) has shown clear linear DNA formation, indicating that it acts as IFP (Interfacial Poisons) which blocks the resealing of the double-stranded DNA (dsDNA). Catenated DNA in the presence of topoisomerase II incubated with compound **10b**, **10g** and **10i** inhibited the topoisomerase II activity represented (lane F, G, H) by the presence of catenated DNA in the well, whereas compound **10b** and **10g** showed clear linear DNA formation similar to etoposide as represented in the well (lane F and G) indicated the inhibition of topo-II.

2.5. Apoptotic studies

2.5.1. Determination of morphological changes

To examine whether the treatment with these compounds could lead to loss of cell viability and induce apoptosis, DU-145 cells were treated with these compounds (**10b**, **10g,** and **10i)**. Cells were observed, and photographs were taken with phase contrast microscope [33]. It can be inferred from Fig. 4, that the treatment with these compounds resulted in reduced number of viable cells in comparison to the vehicle-treated control cells as observed by the distinctive morphological features such as cells detachment from substratum and shrinkage of cells. Even though three compounds have shown morphological effects, compounds **10b** and **10i** had determinant morphological changes compared to the standard VP-16 (Fig. 4).

< **Fig. 4** >

2.5.2. Apoptosis by Hoechst staining

Nuclear fragmentation, chromatin condensation, and nuclear shrinkage are the foremost characteristics of apoptosis. Morphological assessment of these characteristics for apoptosis was performed with Hoechst staining [34]. In our present study, apoptosis-inducing the effect of compounds **VP-16**, **10b**, **10g,** and **10i** where studied in DU-145 cells. Cells treated with compounds **VP-16**, **10b**, **10g,** and **10i** at indicated concentrations for 24 h disclosed the apoptotic characteristics such as condensed and fragmented nuclei. These results revealed that the compounds **VP-16**, **10b**, **10g,** and **10i** were effective in inducing cellular apoptosis (Fig. 5).

< **Fig. 5** >

2.5.3. Measurement of mitochondria membrane potential (ΔΨm)

Mitochondria membrane potential (ΔΨm) was determined by the JC-1 dye. Cells with intact mitochondrion with energized membrane potential shows red aggregates in the presence of JC-1 dye [35]. Potent apoptotic inducers show green fluorescence by losing the membrane potential as de-energized. Cells treated with these compounds **(10b**, **10g,** and **10i)** as well as **VP-16** showed the increased green fluorescence in **VP-16**, **10b,** and **10i** treated cells as compared to untreated (Fig. 6), whereas **10g** has not shown significant green fluorescence in comparison with untreated cell control, indicating that compounds **10b** and **10i** could induce depolarization of mitochondrial membrane potential (Fig. 6).

< **Fig. 6** >

2.5.4. Measurement of reactive oxygen species (ROS)

Accumulation of ROS in the DU-145 cells treated with **VP-16**, **10b**, **10g** and **10i** for 24 h was estimated by 2', 7'– dichlorofluorescein diacetate (DCFDA). It is a non-fluorescent substance and it is converted to 2', 7'–dichlorofluorescein (DCF), inside the cells through oxidation by ROS [36]. Upon treatment with these compounds at indicated concentrations, increased ROS production was observed in dose dependent-manner in comparison to **VP-16**. Whereas compound **10g** has shown equal ROS production and dose dependency was not observed (Fig. 7).

< **Fig. 7** >

2.5.5. Scratch assay

As migration is an important characteristic for metastatic cancers, the effect of these compounds **(10b**, **10g,** and **10i)** on migration of cancer cells was investigated by scratch assay [37]. After 0, 24 and 48 h study revealed that the treatment by **10b** and **10i** resulted in decreased cell migration compared to VP-16. However, compound **10g** did not show any significant decrease in the cell migration (Fig. 8).

< **Fig. 8** >

2.5.6. Annexin V/PI staining assay

Quantification of apoptosis induced by these compounds was determined by using annexin V-FITC-PI staining [38]. This assay is a proven method that differentiates the extent of live, early apoptotic, late apoptotic and necrotic cells as shown in Fig. 9. The percentage of early apoptotic cells in the increased by 6.7% and 7.01% at 0.5 µM whereas 7.0% and 17.65% at 1 µM in comparison to **VP-16** that has shown 4.52% at 2 µM and **10g** did not show any significant increase in the activity. Therefore, these results have proved that the compounds **10b** and **10i** induced apoptosis in a dose-dependent manner (Fig. 9).

< **Fig. 9** >

2.6. Molecular docking study

Cytotoxicity and enzymatic assay results of newly designed podophyllotoxin-triazole conjugates (especially conjugates **10b**, **10g**and **10i**) encouraged us to perform their molecular docking studies at EVP binding pocket of DNA-topoisomerase-IIα to explore the binding pose and protein-small molecule interactions. As similar to co-crystal ligand (EVP), chiral centers present in these conjugates lead to attaining unique conformation to fit well into the binding pocket (Fig. 10A) and showing intercalation with DNA structure present in target protein (Fig. 10B).

< **Fig. 10** >

These conjugates contain aromatic, acyclic ring systems along with a good number of heteroatoms hence they show hydrogen bonding and hydrophobic interactions with the target protein. Interactions shown by these conjugate with target protein are similar due to the similarity in the binding pose. Oxygen atom present in the trimethoxy phenyl ring shows hydrogen bonding (red dashed lines as shown in figure 11A, 11B and 11C) with anamideNHgroup of Asp463. Oxygen atom present in dioxole ring shows hydrogen bonding with side chain NH of Arg487 and amide NH present in these conjugate showing interaction with thecarbonyl oxygen of DG13. In addition, Cl and CF_3 groups present in conjugate **10g** and **10i** respectively are showing interactions with side chain hydroxyl groups of Ser802.

< **Fig. 11** >

In addition to the above mentioned strong interactions, these molecules also show hydrophobic interactions (pink colored region shown in Figure 12A, 12B and 12C) with the target protein. The core tetracyclic ring system present in these conjugates shows

hydrophobic interaction with Arg487, Gly488, DC8, DA12, DG13 residues. Trimethoxy phenyl ring shows interactions with Glu461, Gly462, Asp463, Ser464, Arg487, Gly488, DT9 and DG10. 1-aryl-1*H*-1,2,3-triazole-4-carboxamide motif showing interactions with Met762, Ser802, Pro803, DT9, DC11, DA12.

< **Fig. 12** >

3. Conclusion

In summary, we have designed and synthesized a series of 4*β*-amidotriazole linked podophyllotoxin derivatives (**10a-i** and **11a-k**) and examined their cytotoxicity on six human cancer cell lines. The antiproliferative activity results indicated that most of these compounds exhibit significant inhibitory activities. Compounds **10b, 10g** and **10i** showed potent cytotoxic efficacy against the tested human cancer cell lines. Treatment of DU-145 cells with these compounds resulted in G2/M cell cycle arrest. Moreover, they induce apoptosis through depolarization of mitochondrial membrane potential and increased ROS production. The 4β-amidotriazole linked analogues of podophyllotoxin are found to be more potent in inhibiting human DNA topoisomerase-II. Moreover, the molecular docking study provided some insights into the binding mode of the synthesized compounds in the active site of DNA topoisomerase-II. As a result, it could be concluded that these compounds could be considered as interesting lead molecules and further structural modifications may result in promising new anticancer agents against the prostate cancer.

Acknowledgement

V.G.R acknowledges the UGC, New Delhi for the award of research fellowship and authors thankful to CSIR, New Delhi for the financial support under the 12th Five Year Plan projects “Affordable Cancer Therapeutics (ACT)” (CSC0301) & ORIGIN (CSC-108). S.R.B thanks the Department of Science and Technology (DST), Government of India and the Centre Franco-Indien pour la Promotion de la Recherche Avancée (CEFIPRA) for the award of a Raman-Charpak fellowship.

4. Experimental Section

All reagents, starting materials, and solvents were purchased from Aldrich (Sigma-Aldrich, St. Louis, MO, USA) or Alfa Aesar (Johnson Matthey Company, Ward Hill, MA, USA) and used without further purification. Reactions were monitored by TLC, performed on 0.25 mm

silica gel 60-F254 plates, and visualization on TLC was achieved by UV light or using an iodine indicator. Column chromatography was performed using Merck silica gel of 60-120 mm with hexane and ethyl acetate as eluents. ^{1}H and ^{13}C NMR spectra were recorded with 75, 100, 300, 400, and 500 MHz (AVANCE) spectrometer in $CDCl_3$ and DMSO-d_6 solutions. Chemical shifts (δ) are expressed in ppm relative to the internal standard TMS and multiplicities of NMR signals are represented as singlet (s), broad singlet (bs), doublet (d), triplet (t), double doublet (dd), triplet (t), q (quartet), and multiplets (m). High-resolution mass spectra (ESI-HRMS) were obtained by using ESI-QTOF mass spectrometer (70 eV). Melting points were determined on an electro thermal melting point apparatus and are uncorrected.

4.1. General Procedure for the synthesis of aryl/aliphatic triazolic carboxylic acids (6a-i and 7a-k)

The aryl/aliphatic triazolic carboxylic acids (**6a-i** and **7a-k**) were synthesized based on a literature method as following: By using click chemistry protocol method from the literature, the triazolic esters (**4a-i** and **5a-k**) were synthesized with ethyl propiolate (**3**) and corresponding azides (**2a-i** and **3a-k**). Than after, $LiOH \cdot H_2O$ (1.5 mmol) was added in one portion to a solution of ester (**4a-i** and **5a-k**, 1 mmol) in THF/water (1:1, 20 mL). The reaction mixture was stirred until the solid had dissolved and was then left overnight at room temperature. The solvents were removed in vacuo, and the residue was dissolved in water (15 mL). The resulting solution was washed with diethyl ether (7 mL). The aqueous layer was concentrated to half of its volume and then acidified with 30% hydrochloric acid (15 mL). The resulting precipitate was filtered and dried to give compounds **6a-i** and **7a-k** as a solid with good yields (80-90%). The spectroscopic data of the obtained triazolic acid compounds was in agreement with the reported data [39] and few compounds are reporting for the first time in the present work.

4.1.1. 1-(3,4-dimethoxyphenyl)-1*H*-1,2,3-triazole-4-carboxylic acid (6c)

Light brown solid, yield 82%, Mp: 194-196 ºC; ^{1}H NMR (300 MHz, $CDCl_3$+DMSO-d_6): δ 8.87 (s, 1H), 7.45 (d, J = 2.47 Hz, 1H), 7.38 (dd, J = 2.47, 8.80 Hz, 1H), 7.03 (d, J = 8.80 Hz, 1H), 3.96 (s, 3H), 3.93 (s, 3H). ^{13}C NMR (75 MHz, $CDCl_3$+DMSO-d_6): δ 161.4, 149.1, 148.9, 140.3, 129.4, 125.9, 112.1, 111.2, 104.4, 55.7, 55.5; MS (ESI): *m/z* 250 $[M+H]^+$. HRMS (ESI) calcd for $C_{11}H_{11}O_4N_3$ $[M+H]^+$ 250.08223; found: 250.08358.

4.1.2. 1-(3,5-dimethoxyphenyl)-1*H*-1,2,3-triazole-4-carboxylic acid (6d)

Light brown solid, yield 88%, Mp: 192-194 ºC; ^{1}H NMR (300 MHz, $CDCl_3$+DMSO-d_6): δ 8.61 (s, 1H), 6.94 (s, 2H), 6.53 (s, 1H), 3.87 (s, 6H). ^{13}C NMR (75 MHz, $CDCl_3$+DMSO-d_6): δ 161.6, 161.1, 140.6, 137.4, 125.8, 100.6, 98.6, 55.4; MS (ESI): *m/z* 250 $[M+H]^+$. HRMS (ESI) calcd for $C_{11}H_{11}O_4N_3$ $[M+H]^+$ 250.08223; found: 250.08356.

4.1.3. 1-(3,4,5-trimethoxyphenyl)-1*H*-1,2,3-triazole-4-carboxylic acid (6e)

Off white solid, yield 83%, Mp: 187-189 ºC; ^{1}H NMR (300 MHz, $CDCl_3$+DMSO-d_6): δ 8.80 (s, 1H), 7.09 (s, 2H), 3.95 (s, 6H), 3.87 (s, 3H). ^{13}C NMR (75 MHz, $CDCl_3$+DMSO-d_6): δ 161.4, 153.2, 140.3, 137.6, 131.7, 126.0, 97.8, 60.1, 55.9; MS (ESI): *m/z* 280 $[M+H]^+$. HRMS (ESI) calcd for $C_{12}H_{13}O_5N_3$ $[M+H]^+$ 280.09280; found: 280.09443.

4.1.4. 1-(benzo[*d*][1,3]dioxol-5-yl)-1*H*-1,2,3-triazole-4-carboxylic acid (6f)

Brown solid, yield 86%, Mp: 175-177 ºC; ^{1}H NMR (300 MHz, $CDCl_3$+DMSO-d_6): δ 8.56 (s, 1H), 7.34-7.30 (m, 1H), 7.26-7.20 (m, 1H), 6.95 (m, 1H), 6.12 (s, 2H). ^{13}C NMR (75 MHz, $CDCl_3$+DMSO-d_6): δ 161.6, 148.1, 147.9, 140.5, 130.2, 125.3, 113.9, 108.0, 102.1, 101.6; MS (ESI): *m/z* 234 $[M+H]^+$. HRMS (ESI) calcd for $C_{10}H_7O_4N_3$ $[M+H]^+$ 234.05093; found: 234.05221.

4.1.5. 1-(4-(trifluoromethyl)phenyl)-1*H*-1,2,3-triazole-4-carboxylic acid (6i)

Pale brown solid, yield 81%, Mp: 180-182 ºC; ^{1}H NMR (300 MHz, $CDCl_3$+DMSO-d_6): δ 8.92 (s, 1H), 8.06 (d, J = 8.52 Hz, 2H), 7.85 (d, J = 8.52 Hz, 2H). ^{13}C NMR (75 MHz, $CDCl_3$+DMSO-d_6): δ 161.4, 141.1, 138.5, 126.8 (d, J_{CF3} = 3.30 Hz), 125.4, 121.2, 120.3. MS (ESI): *m/z* 258 $[M+H]^+$. HRMS (ESI) calcd for $C_{10}H_6O_2N_3F_3$ $[M+H]^+$ 258.04849; found: 258.04992.

4.1.6. 1-(3,4-dimethoxybenzyl)-1*H*-1,2,3-triazole-4-carboxylic acid (7d)

White solid, yield 90%, Mp: 196-198 ºC; ^{1}H NMR (300 MHz, $CDCl_3$+DMSO-d_6): δ 7.99 (s, 1H), 6.94-6.80 (m, 3H), 5.51 (s, 2H), 3.88 (s, 3H), 3.85 (s, 3H). ^{13}C NMR (75 MHz, $CDCl_3$+DMSO-d_6): δ 161.6, 148.9, 148.8, 140.2, 126.9, 126.0, 111.0, 55.4, 53.5; MS (ESI): *m/z* 264 $[M+H]^+$. HRMS (ESI) calcd for $C_{12}H_{13}O_4N_3$ $[M+H]^+$ 264.09788; found: 264.09895.

4.1.7. 1-(3,5-dimethoxybenzyl)-1H-1,2,3-triazole-4-carboxylic acid (7e)

White solid, yield 88%, Mp: 186-188 ºC; ^{1}H NMR (300 MHz, $CDCl_3$+DMSO-d_6): δ 7.96 (s, 1H), 6.37-6.26 (m, 3H), 5.42 (s, 2H), 3.71 (s, 6H). ^{13}C NMR (75 MHz, $CDCl_3$+DMSO-d_6): δ 159.9, 135.1, 130.0, 127.2, 120.1, 114.2, 113.5, 55.0, 54.0; MS (ESI): *m/z* 264 $[M+H]^+$. HRMS (ESI) calcd for $C_{12}H_{13}O_4N_3$ $[M+H]^+$ 264.09788; found: 264.09922.

4.1.8. 1-(benzo[*d*][1,3]dioxol-4-ylmethyl)-1*H*-1,2,3-triazole-4-carboxylic acid (7g)

White solid, yield 85%, Mp: 170-172 ºC; ^{1}H NMR (300 MHz, $CDCl_3$+DMSO-d_6): δ 8.13 (s, 1H), 6.88-6.78 (m, 3H), 5.99 (s, 2H), 5.48 (s, 2H). MS (ESI): *m/z* 248 $[M+H]^+$. HRMS (ESI) calcd for $C_{11}H_9O_4N_3$ $[M+H]^+$ 248.06658; found: 248.06780.

4.1.9. 1-(4-(trifluoromethyl)benzyl)-1*H*-1,2,3-triazole-4-carboxylic acid (7j)

Pale brown solid, yield 80%, Mp: 193-195 ºC; ^{1}H NMR (300 MHz, $CDCl_3$+DMSO-d_6): δ 8.15 (s, 1H), 7.65 (d, *J* = 7.97 Hz, 2H), 7.43 (d, *J* = 7.97 Hz, 2H), 5.68 (s, 2H). MS (ESI): *m/z* 272 $[M+H]^+$. HRMS (ESI) calcd for $C_{11}H_8O_2N_3F_3$ $[M+H]^+$ 272.06414; found: 272.06541.

4.2. General Procedure for the synthesis of 4*β*-amido triazole linked derivatives (10a-i and 11a-k)

To a solution of aryl/aliphatic triazolic carboxylic acid (**6a-i** and **7a-k**, 0.5mmol) in anhydrous dimethylformamide, EDCI (0.6 mmol) and HOBT (0.6 mmol) were added at 0 °C and the reaction mixture was stirred for 20 min. To the reaction mixture 4*β*-amino phodophyllotoxin (**9**, 0.5 mmol) was added and stirred at room temperature for 12 h. The contents of the reaction mixture were poured into ice-cold water (25 mL), extracted with ethyl acetate (3x15 mL) and the combined organic phase was washed with brine, dried over anhydrous sodium sulfate, filtered and concentrated in vacuo. The obtained residue was purified by column chromatography using ethyl acetate–hexane (10-50%) as eluent to give analytically pure compounds (**10a-i** and **11a-k**) with finest yields (75-90%).

4.2.1. *N*-((5*S*,5a*S*,8a*R*,9*R*)-8-oxo-9-(3,4,5-trimethoxyphenyl)-5,5a,6,8,8a,9 hexahydrofuro[3',4':6,7]naphtho[2,3-*d*][1,3]dioxol-5-yl)-1-phenyl-1*H*-1,2,3-triazole-4-carboxamide (10a)

White solid, yield 88%, Mp: 170-172 ºC.; $[\alpha]^{25}_{D}$: -86.0 (c: 3.6, $CHCl_3$); ^{1}H NMR (300 MHz, $CDCl_3$): δ 8.54 (s, 1H), 7.76 (d, *J* = 7.55, 2H), 7.64-7.50 (m, 5H), 6.84 (s, 1H), 6.49 (s, 1H), 5.99 (d, *J* = 3.5 Hz, 2H), 5.45 (dd, *J* = 3.39, 7.16 Hz, 1H), 4.58 (d, *J* = 3.21 Hz, 1H), 4.49 (t, *J*

= 6.79 Hz, 1H), 3.98 (d, *J* = 8.87 Hz, 1H), 3.81 (s, 3H), 3.75 (s, 6H), 3.10 (d, *J* = 3.02 Hz, 2H). ^{13}C NMR (100 MHz, $CDCl_3$): *δ* 174.2, 159.7, 152.5, 148.4, 147.5, 142.8, 137.1, 136.2, 134.7, 133.4, 132.3, 130.1, 129.6, 128.2, 123.6, 120.5, 109.6, 108.0, 101.7, 68.8, 60.7, 56.1, 54.6, 48.1, 43.6, 41.5, 37.5; MS (ESI): *m/z* 585 $[M+H]^+$. HRMS (ESI) calcd for $C_{31}H_{28}O_8N_4Na$ $[M+Na]^+$ 607.1805; found: 607.1805.

4.2.2. 1-(4-methoxyphenyl)-*N*-((5*S*,5a*S*,8a*R*,9*R*)-8-oxo-9-(3,4,5-trimethoxyphenyl)-5,5a,6,8,8a,9-hexahydrofuro[3',4':6,7]naphtho[2,3-*d*][1,3]dioxol-5-yl)-1*H*-1,2,3-triazole-4-carboxamide (10b)

White solid, yield 85%, Mp: 195-197 ºC.; $[\alpha]^{25}_D$: -77.6 (c: 3.2, $CHCl_3$); ^{1}H NMR (500 MHz, $CDCl_3$): *δ* 8.43 (s, 1H), 7.65 (d, *J* = 9.0 Hz, 2H), 7.58 (d, *J* = 7.47 Hz, 1H), 7.08 (d, *J* = 9.0 Hz, 2H), 6.84 (s, 1H), 6.47 (s, 1H), 6.29 (s, 2H), 6.00 (d, *J* = 6.56 Hz, 1H), 5.45 (dd, *J* = 4.12, 7.47 Hz, 1H), 4.57 (d, *J* = 4.57 Hz, 1H), 4.49 (dd, *J* = 7.17, 9.30 Hz, 1H), 3.95 (t, *J* = 10.07 Hz, 1H), 3.89 (s, 3H), 3.81 (s, 3H), 3.75 (s, 6H), 3.11-3.03 (m, 2H). ^{13}C NMR (100 MHz, $CDCl_3$): *δ* 174.2, 160.4, 159.8, 152.5, 148.4, 147.5, 142.5, 137.1, 134.7, 132.3, 129.5, 128.2, 123.6, 122.1, 115.0, 109.7, 109.1, 108.0, 101.6, 68.8, 60.7, 56.1, 55.6, 48.1, 43.6, 41.5, 37.5; MS (ESI): *m/z* 615 $[M+H]^+$. HRMS (ESI) calcd for $C_{32}H_{30}O_9N_4Na$ $[M+Na]^+$ 637.1910; found: 637.1909.

4.2.3. 1-(3,4-dimethoxyphenyl)-*N*-((5*S*,5a*S*,8a*R*,9*R*)-8-oxo-9-(3,4,5-trimethoxyphenyl)-5,5a,6,8,8a,9-hexahydrofuro[3',4':6,7]naphtho[2,3-*d*][1,3]dioxol-5-yl)-1*H*-1,2,3-triazole-4-carboxamide (10c)

White solid, yield 84%, Mp: 158-160 ºC.; $[\alpha]^{25}_D$: -84.6 (c: 4.7, $CHCl_3$); ^{1}H NMR (500 MHz, $CDCl_3$): *δ* 8.46 (s, 1H), 7.69 (s, 1H), 7.36 (s, 1H), 7.21 (dd, J = 2.44, 8.54 Hz, 1H), 7.01 (d, *J* = 8.69 Hz, 1H), 6.85 (s, 1H), 6.43 (d, *J* = 4.73 Hz, 1H), 6.28 (s, 2H), 6.00 (q, *J* = 1.37, 3.66 Hz, 2H), 5.45 (dd, *J* = 4.42, 7.32 Hz, 1H), 4.53 (d, *J* = 4.57 Hz, 1H), 4.49 (dd, *J* = 7.47, 9.00 Hz, 1H), 4.00 (s, 3H), 3.97 (s, 3H), 3.94 (d, J = 3.46 Hz, 1H), 3.81 (s, 3H), 3.75 (s, 6H), 3.18-3.12 (m, 1H), 3.10-3.02 (m, 1H). ^{13}C NMR (100 MHz, $CDCl_3$): *δ* 174.3, 159.7, 152.5, 150.1, 150.0, 148.3, 147.4, 142.6, 137.0, 134.7, 132.2, 129.6, 128.2, 123.3, 112.0, 111.3, 109.3, 109.1, 107.9, 104.1, 101.7, 68.8, 60.7, 56.3, 56.2, 56.0, 48.2, 43.6, 41.4, 37.5; MS (ESI): *m/z* 645 $[M+H]^+$. HRMS (ESI) calcd for $C_{33}H_{32}O_{10}N_4Na$ $[M+Na]^+$ 667.2016; found: 667.2019.

4.2.4. 1-(3,5-dimethoxyphenyl)-*N*-((5*S*,5a*S*,8a*R*,9*R*)-8-oxo-9-(3,4,5-trimethoxyphenyl)-5,5a,6,8,8a,9-hexahydrofuro[3',4':6,7]naphtho[2,3-*d*][1,3]dioxol-5-yl)-1*H*-1,2,3-triazole-4-carboxamide (10d)

White solid, yield 87%, Mp: 145-148 ºC.; $[\alpha]^{25}_{D}$: -78.7 (c: 3.8, $CHCl_3$);^{1}H NMR (500 MHz, $CDCl_3$): δ 8.51 (s, 1H), 7.71 (d, *J* = 7.47 Hz, 1H), 6.92 (d, *J* = 2.13 Hz, 2H), 6.84 (s, 1H), 6.58 (t, *J* = 2.13 Hz, 1H), 6.42 (s, 1H), 6.28 (s, 2H), 6.00 (d, *J* = 2.44 Hz, 2H), 5.45 (dd, *J* = 4.42, 7.47 Hz, 1H), 4.54 (d, *J* = 4.88 Hz, 1H), 4.49 (q, *J* = 7.47, 9.00 Hz, 1H), 3.94 (t, *J* = 9.46 Hz, 1H), 3.89 (s, 6H), 3.81 (s, 3H), 3.75 (s, 6H), 3.16 (dd, *J* = 5.18, 14.34 Hz, 1H), 3.10-3.02 (m, 1H). ^{13}C NMR (100 MHz, $CDCl_3$): δ 174.3, 161.7, 159.6, 152.5, 148.4, 147.4, 142.6, 137.6, 137.0, 134.7, 132.2, 128.1, 123.7, 109.4, 109.1, 107.9, 101.7, 101.3, 68.8, 60.7, 56.1, 55.8, 48.2, 43.6, 41.5, 37.5; MS (ESI): *m/z* 645 $[M+H]^+$. HRMS (ESI) calcd for $C_{33}H_{32}O_{10}N_4Na$ $[M+Na]^+$ 667.2016; found: 667.2017.

4.2.5. *N*-((5*S*,5a*S*,8a*R*,9*R*)-8-oxo-9-(3,4,5-trimethoxyphenyl)-5,5a,6,8,8a,9-hexahydrofuro[3',4':6,7]naphtho[2,3-*d*][1,3]dioxol-5-yl)-1-(3,4,5-trimethoxyphenyl)-1*H*-1,2,3-triazole-4-carboxamide (10e)

White solid, yield 89%, Mp: 181-183 ºC.; $[\alpha]^{25}_{D}$: -83.1 (c: 5.9, $CHCl_3$); ^{1}H NMR (500 MHz, $CDCl_3$): δ 8.49 (s, 1H), 7.69 (d, *J* = 7.47 Hz, 1H), 6.97 (s, 2H), 6.85 (s, 1H), 6.43 (s, 1H), 6.28 (s, 2H), 6.01 (q, *J* = 1.37, 2.13 Hz, 2H), 5.45 (dd, *J* = 4.42, 7.47 Hz, 1H), 4.55 (d, *J* = 4.88 Hz, 1H), 4.49 (q, *J* = 7.47, 9.15 Hz, 1H), 3.97 (s, 6H), 3.94 (d, *J* = 1.37 Hz, 1H), 3.91 (s, 3H), 3.81 (s, 3H), 3.75 (s, 6H), 3.15 (dd, *J* = 4.88, 14.34 Hz, 1H), 3.11-3.03 (m, 1H). ^{13}C NMR (100 MHz, $CDCl_3$): δ 174.3, 159.6, 154.1, 152.5, 148.4, 147.4, 142.7, 138.9, 137.1, 134.6, 132.3, 131.8, 128.1, 123.6, 105.9, 109.1, 108.0, 101.7, 97.9, 68.8, 61.0, 60.7, 56.5, 56.1, 54.6, 48.2, 43.7, 41.5, 37.5; MS (ESI): *m/z* 675 $[M+H]^+$. HRMS (ESI) calcd for $C_{34}H_{34}O_{11}N_4Na$ $[M+Na]^+$ 697.2122; found: 697.2116.

4.2.6. 1-(benzo[d][1,3]dioxol-5-yl)-*N*-((5*S*,5a*S*,8a*R*,9*R*)-8-oxo-9-(3,4,5-trimethoxyphenyl)-5,5a,6,8,8a,9-hexahydrofuro[3',4':6,7]naphtho[2,3-*d*][1,3]dioxol-5-yl)-1*H*-1,2,3-triazole-4-carboxamide (10f)

White solid, yield 79%, Mp: 188-191 ºC.; $[\alpha]^{25}_{D}$: -54.6 (c: 4.6, $CHCl_3$); ^{1}H NMR (300 MHz, $CDCl_3$): δ 8.42 (s, 1H), 7.46 (d, *J* = 7.45 Hz, 1H), 7.23 (d, *J* = 2.07 Hz, 1H), 7.16 (dd, *J* = 2.07, 8.31 Hz, 1H), 6.95 (d, *J* = 8.31 Hz, 1H), 6.82 (s, 1H), 6.54 (s, 1H), 6.32 (s, 2H), 6.11 (s, 2H), 5.99 (d, *J* = 7.21 Hz, 2H), 5.45 (dd, *J* = 2.81, 6.96 Hz, 1H), 4.64 (d, *J* = 2.07 Hz, 1H),

4.52-4.46 (m, 1H), 3.97-3.91 (m, 1H), 3.82 (s, 3H), 3.76 (s, 6H), 3.09-3.05 (m, 2H). ^{13}C NMR (100 MHz, $CDCl_3$): δ 174.2, 159.7, 152.5, 148.8, 148.7, 148.4, 147.5, 142.5, 137.1, 134.7, 132.3, 130.6, 128.2, 123.9, 114.4, 109.8, 109.1, 108.7, 108.1, 102.5, 102.3, 101.6, 68.8, 60.6, 56.1, 48.1, 43.7, 41.6, 37.5; MS (ESI): *m/z* 629 $[M+H]^+$. HRMS (ESI) calcd for $C_{32}H_{28}O_{10}N_4Na$ $[M+Na]^+$ 651.1703; found: 651.1703.

4.2.7. 1-(4-chlorophenyl)-*N*-((5*S*,5a*S*,8a*R*,9*R*)-8-oxo-9-(3,4,5-trimethoxyphenyl)-5,5a,6,8,8a,9-hexahydrofuro[3',4':6,7]naphtho[2,3-*d*][1,3]dioxol-5-yl)-1*H*-1,2,3-triazole-4-carboxamide (10g)

White solid, yield 83%, Mp: 222-225 ºC.; $[\alpha]^{25}_D$: -72.5 (c: 1.2, $CHCl_3$); ^{1}H NMR (500 MHz, $CDCl_3$): δ 8.52 (s, 1H), 7.72 (d, *J* = 8.85 Hz, 2H), 7.57 (d, *J* = 8.85 Hz, 2H), 7.52 (d, *J* = 7.47 Hz, 1H), 6.83 (s, 1H), 6.51 (s, 1H), 6.30 (s, 2H), 6.00 (d, *J* = 7.47 Hz, 2H), 5.45 (dd, *J* = 3.35, 7.47 Hz, 1H), 4.60 (d, *J* = 3.35 Hz, 1H), 4.51-4.47 (m, 1H), 3.96-3.91 (m, 1H), 3.81 (s, 3H), 3.76 (s, 6H), 3.08-3.04 (m, 2H). ^{13}C NMR (100 MHz, $CDCl_3$): δ 174.1, 159.7, 152.5, 148.4, 147.6, 142.6, 137.1, 135.3, 134.7, 132.3, 131.9, 129.5, 128.2, 125.5, 109.8, 109.1, 108.1, 101.6, 68.8, 60.7, 56.1, 53.8, 47.9, 43.7, 41.6, 37.5; MS (ESI): *m/z* 619 $[M+H]^+$. HRMS (ESI) calcd for $C_{31}H_{27}O_8N_4ClNa$ $[M+Na]^+$ 641.1415; found: 641.1417.

4.2.8. 1-(4-fluorophenyl)-*N*-((5*S*,5a*S*,8a*R*,9*R*)-8-oxo-9-(3,4,5-trimethoxyphenyl)-5,5a,6,8,8a,9-hexahydrofuro[3',4':6,7]naphtho[2,3-*d*][1,3]dioxol-5-yl)-1*H*-1,2,3-triazole-4-carboxamide (10h)

White solid, yield 81%, Mp: 228-230 ºC.; $[\alpha]^{25}_D$: -52.8 (c: 3.5, $CHCl_3$); ^{1}H NMR (400 MHz, $CDCl_3$): δ 8.49 (s, 1H), 7.74 (dd, *J* = 4.52, 8.92 Hz, 2H), 7.49 (s, 1H), 7.31-7.27 (m, 2H), 6.83 (s, 1H), 6.55-6.51 (s, 1H), 6.31 (s, 2H), 5.99 (dd, *J* = 1.22, 7.21 Hz, 2H), 5.45 (dd, *J* = 3.30, 7.45 Hz, 1H), 4.62 (s, 1H), 4.51-4.46 (m, 1H), 3.98-3.91 (m, 1H),), 3.82 (s, 3H), 3.76 (s, 6H), 3.10-3.04 (m, 2H). ^{13}C NMR (100 MHz, $CDCl_3$): δ 174.1, 162.9 (d, J_{CF} = 250.8 Hz), 159.6, 152.5, 148.4, 147.6, 142.8, 137.1, 134.6, 132.5 (d, J_{CF} = 2.9 Hz), 132.3, 128.1, 123.8, 122.6 (d, J_{CF} = 8.0 Hz), 117.1 (d, J_{CF} = 22.7 Hz), 109.8, 109.1, 108.0, 101.6, 68.8, 60.7, 56.1, 48.1, 43.7, 41.6, 37.5; HRMS (ESI) calcd for $C_{31}H_{27}O_8N_4FNa$ $[M+Na]^+$ 625.1711; found: 625.1717.

4.2.9. *N*-((5*S*,5a*S*,8a*R*,9*R*)-8-oxo-9-(3,4,5-trimethoxyphenyl)-5,5a,6,8,8a,9-hexahydrofuro[3',4':6,7]naphtho[2,3-*d*][1,3]dioxol-5-yl)-1-(4-(trifluoromethyl)phenyl)-1*H*-1,2,3-triazole-4-carboxamide (10i)

White solid, yield 79%, Mp: 190-194 ºC.; $[\alpha]^{25}_{D}$: -93.6 (c: 3.9, $CHCl_3$); ^{1}H NMR (400 MHz, $CDCl_3$): δ 8.62 (s, 1H), 7.93 (d, *J* = 8.55 Hz, 2H), 7.87 (d, *J* = 8.55 Hz, 2H), 7.47 (d, *J* = 7.45 Hz, 1H), 6.83 (s, 1H), 6.55 (s, 1H), 6.32 (s, 2H), 6.01-5.97 (m, 2H), 5.47 (dd, *J* = 3.42, 7.33 Hz, 1H), 4.64 (d, *J* = 4.89 Hz, 1H), 4.52-4.41 (m, 2H), 3.97-3.91 (m, 1H), 3.82 (s, 3H), 3.76 (s, 6H), 3.10-3.04 (m, 2H). ^{13}C NMR (100 MHz, $CDCl_3$): δ 174.2, 159.4, 152.5, 148.5, 147.6, 143.1, 138.6, 137.2, 134.6, 132.4, 128.2, 128.1, 127.4, 123.7,120.7,110.0, 109.1, 108.1, 101.6, 69.0, 68.8, 60.6, 56.1, 48.1, 43.7, 41.7, 37.4; MS (ESI): *m/z* 653 $[M+H]^+$. HRMS (ESI) calcd for $C_{32}H_{27}O_8N_4F_3Na$ $[M+Na]^+$ 675.1679; found: 675.1677.

4.2.10. 1-benzyl-*N*-((5*S*,5a*S*,8a*R*,9*R*)-8-oxo-9-(3,4,5-trimethoxyphenyl)-5,5a,6,8,8a,9-hexahydrofuro[3',4':6,7]naphtho[2,3-*d*][1,3]dioxol-5-yl)-1*H*-1,2,3-triazole-4-carboxamide (11a)

White solid, yield 80%, Mp: 164-166 ºC.; $[\alpha]^{25}_{D}$: -97.5 (c: 5.5, $CHCl_3$); ^{1}H NMR (500 MHz, $CDCl_3$): δ 7.99 (s, 1H), 7.42-7.39 (m, 4H), 7.32-7.29 (m, 2H), 6.78 (s, 1H), 6.53 (s, 1H), 6.31 (s, 2H), 5.98 (dd, *J* = 1.22, 10.33 Hz, 2H), 5.57 (s, 2H), 5.40 (dd, *J* = 3.66, 7.47 Hz, 1H), 4.63 (d, *J* = 3.66 Hz, 1H), 4.46-4.42 (m, 1H), 3.89 (t, *J* = 9.15 Hz, 1H), 3.81 (s, 3H), 3.75 (s, 6H), 3.05-3.02 (m, 2H). ^{13}C NMR (100 MHz, $CDCl_3$): δ 174.2, 159.8, 152.5, 148.4, 147.5, 142.4, 137.1, 134.7, 133.4, 132.3, 129.3, 129.2, 128.2, 125.5, 109.9, 109.1, 108.0, 101.6, 68.8, 60.7, 56.1, 54.6, 47.9, 43.6, 41.6, 37.5; MS (ESI): *m/z* 599 $[M+H]^+$. HRMS (ESI) calcd for $C_{32}H_{30}O_8N_4Na$ $[M+Na]^+$ 621.1961; found: 621.1963.

4.2.11. 1-(4-methoxybenzyl)-*N*-((5*S*,5a*S*,8a*R*,9*R*)-8-oxo-9-(3,4,5-trimethoxyphenyl)-5,5a,6,8,8a,9-hexahydrofuro[3',4':6,7]naphtho[2,3-*d*][1,3]dioxol-5-yl)-1*H*-1,2,3-triazole-4-carboxamide (11b)

White solid, yield 84%, Mp: 174-177 ºC.; $[\alpha]^{25}_{D}$: -72.55 (c: 7.6, $CHCl_3$); ^{1}H NMR (500 MHz, $CDCl_3$): δ 7.95 (s, 1H), 7.60 (d, *J* = 7.55 Hz, 1H), 7.28 (d, *J* = 1.88 Hz, 1H), 7.25 (s, 1H), 6.93 (d, *J* = 8.68 Hz, 2H), 6.80 (s, 1H), 6.44 (s, 1H), 6.30 (s, 2H), 5.98 (d, *J* = 4.72 Hz, 2H), 5.49 (s, 2H), 5.38 (dd, *J* = 3.77, 7.36 Hz, 1H), 4.5 (d, *J* = 4.15 Hz, 1H), 4.46-4.39 (m, 1H), 3.88 (t, *J* = 9.81 Hz, 2H), 3.81 (s, 6H), 3.75 (s, 6H), 3.06-3.00 (m, 2H). ^{13}C NMR (100 MHz, $CDCl_3$): δ 174.2, 160.2, 159.9, 152.5, 148.4, 147.5, 142.3, 137.1, 134.7, 133.4, 132.3, 129.9, 128.2, 125.3, 114.6, 109.8, 109.1, 108.1, 101.6, 68.8, 60.6, 56.1, 55.3, 54.2, 47.9, 43.6, 41.6, 37.5; MS (ESI): *m/z* 629 $[M+H]^+$. HRMS (ESI) calcd for $C_{33}H_{32}O_9N_4Na$ $[M+Na]^+$ 651.2067; found: 651.2070.

4.2.12. 1-(3-methoxybenzyl)-*N*-((5*S*,5aS,8a*R*,9*R*)-8-oxo-9-(3,4,5-trimethoxyphenyl)-5,5a,6,8,8a,9-hexahydrofuro[3',4':6,7]naphtho[2,3-*d*][1,3]dioxol-5-yl)-1*H*-1,2,3-triazole-4-carboxamide (11c)

White solid, yield 83%, Mp: 165-168 ºC.; $[\alpha]^{25}_{D}$: -78.0 (c: 5.5, $CHCl_3$); ^{1}H NMR (500 MHz, $CDCl_3$): δ 8.00 (s, 1H), 7.37 (d, *J* = 7.47 Hz, 1H), 7.32 (t, *J* = 7.93 Hz, 1H), 6.92 (dd, *J* = 2.44, 8.39 Hz, 1H), 6.88 (d, *J* = 7.62 Hz, 1H), 6.82 (t, *J* = 1.98 Hz, 1H), 6.78 (s, 1H), 6.54 (s, 1H), 6.31 (s, 2H), 5.98 (dd, *J* = 1.37, 10.98 Hz, 2H), 5.53 (s, 2H), 5.40 (dd, *J* = 3.81, 7.62 Hz, 1H), 4.63 (d, *J* = 3.96 Hz, 1H), 4.46-4.42 (m, 1H), 3.89 (t, *J* = 9.15 Hz, 1H), 3.81 (s, 3H), 3.80 (s, 3H), 3.75 (s, 6H), 3.05-3.01 (m, 2H). ^{13}C NMR (100 MHz, $CDCl_3$): δ 174.2, 160.1, 159.8, 152.5, 148.4, 147.6, 142.4, 137.1, 134.7, 132.3, 130.4, 128.2, 125.6, 120.4, 114.4, 114.1, 109.9, 109.1, 108.1, 101.6, 68.8, 60.7, 56.1, 55.3, 54.5, 47.9, 43.6, 41.6, 37.5; MS (ESI): *m/z* 629 $[M+H]^+$. HRMS (ESI) calcd for $C_{33}H_{32}O_9N_4Na$ $[M+Na]^+$ 651.2067; found: 651.2064.

4.2.13. 1-(3,4-dimethoxybenzyl)-*N*-((5*S*,5a*S*,8a*R*,9*R*)-8-oxo-9-(3,4,5-trimethoxyphenyl)-5,5a,6,8,8a,9-hexahydrofuro[3',4':6,7]naphtho[2,3-*d*][1,3]dioxol-5-yl)-1*H*-1,2,3-triazole-4-carboxamide (11d)

White solid, yield 88%, Mp: 180-183 ºC.; $[\alpha]^{25}_{D}$: -59.6 (c: 5.6, $CHCl_3$); ^{1}H NMR (500 MHz, $CDCl_3$): δ 7.98 (s, 1H), 7.40 (t, *J* = 7.32 Hz, 1H), 6.90 (d, *J* = 1.90 Hz, 1H), 6.88 (s, 1H), 6.82 (d, *J* = 1.98 Hz, 1H), 6.78 (s, 1H), 6.53 (d, *J* = 3.66, 1H), 6.31 (s, 2H), 5.98 (dd, *J* = 1.22, 10.22 Hz, 2H), 5.49 (s, 2H), 5.39 (dd, *J* = 3.50, 7.47 Hz, 1H), 4.63 (s, 1H), 4.46-4.42 (m, 1H), 3.89 (s, 3H), 3.87 (s, 3H), 3.81 (s, 3H), 3.75 (s, 6H), 3.05-3.01 (m, 2H). ^{13}C NMR (100 MHz, $CDCl_3$): δ 174.2, 159.9, 152.5, 149.8, 149.5, 148.4, 147.4, 142.3, 137.1, 134.7, 132.3, 128.2, 125.6, 125.3, 121.2, 111.4, 111.3, 109.9, 109.1, 108.1, 101.6, 68.8, 60.7, 56.1, 55.9, 54.6, 47.9, 43.6, 41.6, 37.5; MS (ESI): *m/z* 659 $[M+H]^+$. HRMS (ESI) calcd for $C_{34}H_{34}O_{10}N_4Na$ $[M+Na]^+$ 681.2173; found: 651.2167.

4.2.14. 1-(3,5-dimethoxybenzyl)-*N*-((5*S*,5a*S*,8a*R*,9*R*)-8-oxo-9-(3,4,5-trimethoxyphenyl)-5,5a,6,8,8a,9-hexahydrofuro[3',4':6,7]naphtho[2,3-*d*][1,3]dioxol-5-yl)-1*H*-1,2,3-triazole-4-carboxamide (11e)

White solid, yield 86%, Mp: 245-248 ºC.; $[\alpha]^{25}_{D}$: -70.4 (c: 4.5, $CHCl_3$); ^{1}H NMR (500 MHz, $CDCl_3$): δ 8.01 (s, 1H), 7.40 (d, *J* = 7.47 Hz, 1H), 6.79 (s, 1H), 6.53 (s, 1H), 6.46 (s, 1H), 6.42 (s, 2H), 6.31 (s, 2H), 5.98 (d, *J* = 10.22, 2H), 5.47 (s, 2H), 5.40 (dd, *J* = 2.28, 6.71 Hz,

1H), 4.63 (s, 1H), 4.47-4.42 (m, 1H), 3.92-3.87 (m, 1H), 3.81 (s, 3H), 3.78 (s, 6H), 3.75 (s, 6H), 3.06-3.01 (m, 2H). ^{13}C NMR (100 MHz, $CDCl_3$): δ 174.2, 161.4, 159.8, 152.5, 148.4, 147.5, 142.4, 137.1, 135.3, 134.7, 132.3, 128.2, 125.6, 109.9, 109.1, 108.0, 106.3, 101.6, 100.5, 68.8, 60.6, 56.1, 55.4, 54.6, 47.9, 43.6, 41.6, 37.5; MS (ESI): *m/z* 659 $[M+H]^+$. HRMS (ESI) calcd for $C_{34}H_{34}O_{10}N_4Na$ $[M+Na]^+$ 681.2173; found: 651.2173.

4.2.15. *N*-((5*S*,5a*S*,8a*R*,9*R*)-8-oxo-9-(3,4,5-trimethoxyphenyl)-5,5a,6,8,8a,9-hexahydrofuro[3',4':6,7]naphtho[2,3-*d*][1,3]dioxol-5-yl)-1-(3,4,5-trimethoxybenzyl)-1*H*-1,2,3-triazole-4-carboxamide (11f)

White solid, yield 85%, Mp: 189-192 ºC.; $[\alpha]^{25}_D$: -87.9 (c: 6.0, $CHCl_3$); ^{1}H NMR (500 MHz, $CDCl_3$): δ 8.02 (s, 1H), 7.37 (d, *J* = 7.47 Hz, 1H), 6.78 (s, 1H), 6.54 (s, 1H), 6.53 (s, 2H), 6.31 (s, 2H), 5.98 (dd, *J* = 1.22, 10.37 Hz, 2H), 5.47 (s, 2H), 5.40 (dd, *J* = 3.96, 7.47 Hz, 1H), 4.64 (d, *J* = 4.27 Hz, 1H), 4.47-4.43 (m, 1H), 3.90-3.87 (m, 1H), 3.86 (s, 6H), 3.85 (s, 3H), 3.81 (s, 3H), 3.75 (s, 6H), 3.06-3.01 (m, 2H). ^{13}C NMR (100 MHz, $CDCl_3$): δ 174.1, 159.8, 153.8, 152.5, 148.4, 147.6, 142.4, 138.7, 137.1, 134.7, 132.3, 128.6, 128.2, 125.5, 109.9, 109.1, 108.1, 105.6, 101.6, 68.8, 60.8, 60.7, 56.2, 56.1, 55.0, 47.9, 43.6, 41.6, 37.5; MS (ESI): *m/z* 689 $[M+H]^+$. HRMS (ESI) calcd for $C_{35}H_{36}O_{11}N_4Na$ $[M+Na]^+$ 711.2278; found: 711.2267.

4.2.16. 1-(benzo[*d*][1,3]dioxol-5-ylmethyl)-*N*-((5*S*,5a*S*,8a*R*,9*R*)-8-oxo-9-(3,4,5-trimethoxyphenyl)-5,5a,6,8,8a,9-hexahydrofuro[3',4':6,7]naphtho[2,3-*d*][1,3]dioxol-5-yl)-1*H*-1,2,3-triazole-4-carboxamide (11g)

White solid, yield 83%, Mp: 170-173 ºC.; $[\alpha]^{25}_D$: -50.0 (c: 6.9, $CHCl_3$); ^{1}H NMR (500 MHz, $CDCl_3$): δ 7.98 (s, 1H), 7.39 (d, *J* = 7.62 Hz, 1H), 6.82 (d, J = 0.91 Hz, 2H), 6.78 (s, 1H), 6.76 (s, 1H), 6.53 (s, 1H), 6.31 (s, 2H), 5.99 (s, 2H), 5.98 (dd, *J* = 1.37, 11.29 Hz, 2H), 5.46 (s, 2H), 5.40 (dd, *J* = 3.66, 7.47 Hz, 1H), 4.63 (d, *J* = 3.96 Hz, 1H), 4.46-4.42 (m, 1H), 3.91-3.87 (m, 1H), 3.81 (s, 3H), 3.75 (s, 6H), 3.05-3.01 (m, 2H). ^{13}C NMR (100 MHz, $CDCl_3$): δ 174.2, 159.8, 152.5, 148.4, 147.6, 142.4, 137.1, 134.7, 132.3, 128.2, 126.9, 125.4, 122.3, 109.9, 109.1, 108.7, 108.6, 108.1, 101.6, 101.5, 68.8, 60.7, 56.1, 54.5, 47.9, 43.6, 41.6, 37.5; MS (ESI): *m/z* 643 $[M+H]^+$. HRMS (ESI) calcd for $C_{33}H_{30}O_{10}N_4Na$ $[M+Na]^+$ 665.1860; found: 665.1861.

4.2.17. 1-(4-chlorobenzyl)-*N*-((5*S*,5a*S*,8a*R*,9*R*)-8-oxo-9-(3,4,5-trimethoxyphenyl)-5,5a,6,8,8a,9-hexahydrofuro[3',4':6,7]naphtho[2,3-*d*][1,3]dioxol-5-yl)-1*H*-1,2,3-triazole-4-carboxamide (11h)

White solid, yield 78%, Mp: 180-184 ºC.; $[\alpha]^{25}_{D}$: -87.4 (c: 3.7, $CHCl_3$); ^{1}H NMR (400 MHz, $CDCl_3$): δ 8.01 (s, 1H), 7.39 (d, J = 8.43 Hz, 2H), 7.39-7.35 (m, 1H), 7.24 (d, J = 8.43 Hz, 2H), 6.78 (s, 1H), 6.54 (s, 1H), 6.31 (s, 2H), 5.98 (dd, J = 1.2, 8.9 Hz, 2H), 5.54 (s, 2H), 5.40 (dd, J = 3.7, 7.5 Hz, 1H), 5.30 (s, 1H), 4.63 (d, J = 4.03 Hz, 1H), 4.46-4.42 (m, 1H), 3.92-3.86 (m, 1H), 3.81 (s, 3H), 3.75 (s, 6H), 3.06-3.01 (m, 2H). ^{13}C NMR (100 MHz, $CDCl_3$): δ 174.2, 159.7, 152.5, 148.4, 147.6, 142.6, 137.1, 135.3, 134.7, 132.3, 131.9, 129.5, 128.2, 125.5, 109.9, 109.1, 108.1, 101.6, 68.8, 60.6, 56.1, 53.8, 47.9, 43.6, 41.6, 37.4; MS (ESI): *m/z* 633 $[M+H]^+$. HRMS (ESI) calcd for $C_{32}H_{29}O_8N_4ClNa$ $[M+Na]^+$ 655.1572; found: 655.1572.

4.2.18. 1-(4-fluorobenzyl)-*N*-((5*S*,5a*S*,8a*R*,9*R*)-8-oxo-9-(3,4,5-trimethoxyphenyl)-5,5a,6,8,8a,9-hexahydrofuro[3',4':6,7]naphtho[2,3-*d*][1,3]dioxol-5-yl)-1*H*-1,2,3-triazole-4-carboxamide (11i)

White solid, yield 82%, Mp: 169-172 ºC.; $[\alpha]^{25}_{D}$: -76.0 (c: 5.5, $CHCl_3$); ^{1}H NMR (500 MHz, $CDCl_3$): δ 8.00 (s, 1H), 7.38 (d, J = 7.32 Hz, 1H), 7.32-7.29 (m, 2H), 7.10 (t, J = 8.54 Hz, 2H), 6.78 (s, 1H), 6.53 (s, 1H), 6.31 (s, 2H), 5.98 (dd, J = 1.22, 10.98 Hz, 2H), 5.55 (s, 2H), 5.40 (dd, J = 3.81, 7.62 Hz, 1H), 4.63 (d, J = 43.50 Hz, 1H), 4.46-4.42 (m, 1H), 3.91-3.87 (m, 1H), 3.81 (s, 3H), 3.75 (s, 6H), 3.06-3.01 (m, 2H). ^{13}C NMR (100 MHz, $CDCl_3$): δ 174.2, 163.0 (d, J_{CF} = 249.4 Hz), 159.7, 152.5, 148.4, 147.6, 142.5, 137.1, 134.7, 132.3, 130.2 (d, J_{CF} = 8.0 Hz), 129.3 (d, J_{CF} = 2.2 Hz), 128.2, 125.4, 116.4 (d, J_{CF} = 21.2 Hz), 109.9, 109.1, 108.1, 101.6, 68.8, 60.7, 56.1, 53.8, 47.9, 43.6, 41.6, 37.5; MS (ESI): *m/z* 617 $[M+H]^+$. HRMS (ESI) calcd for $C_{32}H_{29}O_8N_4FNa$ $[M+Na]^+$ 639.1867; found: 639.1871.

4.2.19. *N*-((5*S*,5a*S*,8a*R*,9*R*)-8-oxo-9-(3,4,5-trimethoxyphenyl)-5,5a,6,8,8a,9-hexahydrofuro[3',4':6,7]naphtho[2,3-*d*][1,3]dioxol-5-yl)-1-(4-(trifluoromethyl)benzyl)-1*H*-1,2,3-triazole-4-carboxamide (11j)

White solid, yield 80%, Mp: 171-174 ºC.; $[\alpha]^{25}_{D}$: -93.6 (c: 3.9, $CHCl_3$); ^{1}H NMR (500 MHz, $CDCl_3$): δ 8.05 (s, 1H), 7.68 (d, J = 8.08 Hz, 2H), 7.42 (d, J = 8.08 Hz, 2H), 7.37 (d, J = 7.47 Hz, 1H), 6.78 (s, 1H), 6.55 (s, 1H), 6.31 (s, 2H), 5.98 (dd, J = 1.22, 10.98 Hz, 2H), 5.65 (s, 2H), 5.40 (dd, J = 3.96, 7.47 Hz, 1H), 4.64 (d, J = 4.12 Hz, 1H), 4.46-4.43 (m, 1H), 3.92-3.87 (m, 1H), 3.81 (s, 3H), 3.75 (s, 6H), 3.06-3.01 (m, 2H). ^{13}C NMR (100 MHz, $CDCl_3$): δ 174.1,

159.6, 152.5, 148.5, 147.6, 142.7, 137.4, 137.2, 134.7, 132.4, 128.4, 128.2, 126.3 (d, J_{CF3} = 3.6 Hz), 125.7, 110.0, 109.1, 108.1, 101.6, 68.8, 60.7, 56.1, 53.9, 47.9, 43.7, 41.7, 37.5; MS (ESI): *m/z* 667 $[M+H]^+$. HRMS (ESI) calcd for $C_{33}H_{30}O_8N_4F_3$ $[M+H]^+$ 667.2016; found: 667.2013.

4.2.20. *N*-((5*S*,5a*S*,8a*R*,9*R*)-8-oxo-9-(3,4,5-trimethoxyphenyl)-5,5a,6,8,8a,9-hexahydrofuro[3',4':6,7]naphtho[2,3-*d*][1,3]dioxol-5-yl)-1-(3-phenoxybenzyl)-1*H*-1,2,3-triazole-4-carboxamide (11k)

White solid, yield 87%, Mp: 148-151 ºC.; $[\alpha]^{25}_D$: -74.0 (c: 4.9, $CHCl_3$); ^{1}H NMR (500 MHz, $CDCl_3$): δ 8.02 (s, 1H), 7.38-7.33 (m, 4H), 7.16 (t, *J* = 7.47 Hz, 1H), 7.01 (d, *J* = 7.78 Hz, 2H), 6.99 (dd, *J* = 1.98, 8.08 Hz, 2H), 6.94 (s, 1H), 6.79 (s, 1H), 6.54 (s, 1H), 6.32 (s, 2H), 5.98 (d, *J* = 11.44 Hz, 2H), 5.53 (s, 2H), 5.40 (dd, *J* = 3.81, 7.62 Hz, 1H), 4.64 (d, *J* = 4.12 Hz, 1H), 4.47-4.43 (m, 1H), 3.92-3.88 (m, 1H), 3.81 (s, 3H), 3.75 (s, 6H), 3.06-3.02 (m, 2H). ^{13}C NMR (100 MHz, $CDCl_3$): δ 174.1, 159.8, 158.2, 156.1, 152.5, 148.4, 147.5, 142.4, 137.1, 135.2, 134.7, 132.3, 130.6, 129.8, 128.2, 125.6, 123.9, 122.5, 119.3, 118.8, 118.1, 109.9, 109.1, 108.0, 101.6, 68.8, 60.6, 56.1, 54.2, 47.9, 43.6, 41.6, 37.5; MS (ESI): *m/z* 691 $[M+H]^+$. HRMS (ESI) calcd for $C_{38}H_{34}O_9N_4Na$ $[M+Na]^+$ 713.2223; found: 713.2224.

4.4. Biology

4.4.1. Cell culture

The cell lines, Cervical (Hela), Breast (MCF-7), Prostate (DU-145), Lung (A549), Liver (HepG2) and Colon (HT-29) which were used in this study were procured from American Type Culture Collection (ATCC), United States and were maintained in the Dulbecco's modified Eagle's medium containing 10% (v/v) fetal bovine serum (FBS; HyClone, Logan, UT) supplemented with 100 units/mL of penicillin and streptomycin (Sigma-Aldrich, St. Louis, MO). All cells were cultured at 37 ºC in a humidified atmosphere with 5% CO_2. Test compounds were dissolved in DMSO (Sigma-Aldrich) to prepare 10 mM stock solution for the following experiments. The stock was diluted with culture medium to desired concentrations for drug treatment.

4.4.2. Evaluation of anti-proliferative activity

The cytotoxic activity of the compounds was determined by using MTT assay [40]. Cells were seeded in 100 µL DMEM, supplemented with 10% FBS in each well of 96-well microculture plates and incubated for 24 h at 37 ºC in a CO_2 incubator. After incubation cells were treated with test compounds for 48 h. After 48 h of incubation, 10 µL MTT (3-(4,5-dimethylthiazol-2-yl)- 2,5-diphenyl tetrazolium bromide) (5 mg/mL) was added to each well and the plates were further incubated for 4 h. Then the supernatant from each well was carefully removed, formazan crystals were dissolved in 100 µL of DMSO and absorbance at 570 nm wavelength was recorded.

4.4.3. Cell cycle analysis

Effect of compounds **10b**, **10g** and **10i** on DNA content by cell cycle progression was assessed using DU-145 cells. Cells ($2x10^5$/well) were incubating in a 6-well plate with incomplete media (serum free) for 24 h; to bring all cells in a synchronized state [41]. After 24 hrs the incomplete media was replaced with complete media with or without compounds **VP-16**, **10b**, **10g** and **10i** at indicated concentrations and incubated for 24 h. The cells were washed thrice with PBS, harvested, fixed in ice cold PBS in 70% ethanol, and stored at -20 ºC for 30 min. After fixation, these cells were incubated with RNase A (0.1 mg/mL) at 37 ºC for 30 min, stained with propidium iodide (50 µg/mL) for 30 min on ice in dark, and then measured for DNA content using BD FACSVerse flow cytometer (Becton Dickinson, USA).

4.4.4. DNA topoisomerase-II inhibition assay

The topoisomerase II assay was done by the protocol provided by TopoGEN, Inc. The total reaction volume of the topoisomerase II mediated cleavage reaction was fixed at 20 µL. Briefly, assay buffer [50 mM Tris-HCl, pH 8, 120 mM KCl, 10 mM $MgCl_2$, 0.5 mM ATP, 0.5 mM dithiothreitol, 30 µg/mL bovine serum albumin (BSA)] containing 200 ng of KDNA (TOPOgen), and a solution of the test drugs were added to five units of the human recombinant topoisomerase II (the amount of enzyme which resulted in the complete decatenation of 200 ng of KDNA). After 10 min. of incubation at 37 ºC, the reaction was stopped by addition of 5 µL of stop buffer containing the loading dye and then the reaction mixture was analyzed on a 1% agarose gel in TAE buffer.

4.4.5. Determination of morphological changes

Morphological changes were assessed based on the method described by the reported method [42] with slight modifications. DU-145 cells were seeded at a density of $2x10^5$ cells/well in a 6-well plate and incubated overnight. Media was replaced with the fresh media containing the compounds **10b**, **10g** and **10i** at indicated concentrations for 24 h. After incubation morphological changes in the cells were observed under the phase contrast microscope and images were captured with (Olympus-1X71SIF-3), capture 7 pro software.

4.4.6. Apoptosis by Hoechst staining

An apoptotic cell staining was performed according to the literature method [43]. Briefly, DU-145 cells were seeded in to 6-well plate at a density of $1x10^5$ cells/well and incubated for overnight, and media was replaced with fresh media containing with or without compounds **VP-16**, **10b**, **10g** and **10i** at indicated concentrations and further incubated for 24 hrs. Then cells were washed three times with PBS and stained with Hoechst (1 µg/ml) for 20 min at 37 ºC. After incubation cells were washed with PBS three times to remove unstained Hoechst and images were captured with fluorescence microscope (Olympus-1X71SIF-3), capture 7 pro software.

4.4.7. Measurement of mitochondrial membrane potential (ΔΨm)

Mitochondrial membrane potential was measured by according to the manufacturer's protocol BD^{TM} Mitoscreen kit. Briefly, seed $2x10^5$ cells/well in to the 6-well plates and incubate for overnight. Replace the medium with fresh medium containing compounds **VP-16**, **10b**, **10g** and **10i** at indicated concentrations for 24 h. After incubation trypsinise the cells and collect it into 15 mL tubes and centrifuge at 400 g for 5 min at room temperature. Collect the pellet and add 0.5 mL of freshly prepared JC-1 working solution to each pellet and incubate for 15 min at 37 ºC in CO_2 incubator. After incubation wash the cells twice with 1x assay buffer at room temperature. Resuspend the cells in 0.5 mL of 1x assay buffer and analyze by flow cytometry [44].

4.4.8. Measurement of reactive oxygen species (ROS)

ROS production from DU-145 cells treated with compounds **VP-16**, **10b**, **10g** and **10i** was measured using 2',7'–dichlorofluorescin diacetate (DCFDA) dye [24]. DU-145 cells were seeded in a 6-well plate at a density of $2x10^5$ cells/well and incubated for overnight. After incubation media was replaced with fresh medium containing compounds **VP-16**, **10b**, **10g**

and **10i** at indicated concentrations for 24 h. After 24 h medium was replaced with fresh medium containing DCFDA (10 µM) and incubated in dark conditions for 30 min at room temperature. Cells were washed with PBS twice and fluorescence intensity was measured by fluorescence microscope (Olympus-1X71SIF-3), capture 7 prosoftware.

4.4.9. Scratch assay

In vitro scratch assay is used to determine the cell migration and method was adopted from the literature [45]. DU-145 cells were seeded in a 6-well plate at a density of $2x10^5$ cells/well and maintained till confluency. Small scratch was made with sterile 200 µL tip and washed with PBS to remove debris occurred by scratch. Fresh media containing compounds **VP-16**, **10b**, **10g** and **10i** at indicated concentrations was added. Cell migration was monitored with phase contract microscopy and images were captured at 0, 24 and 48 h.

4.4.10. Annexin V/PI staining assay

Annexin V/PI assay was determined using the Annexin V FITC apoptosis detection kit (Sigma Aldrich cat. No: APOAF) [46]. Briefly, cells were seeded in 6-well plate at a density of $1×10^5$ cells/well and allowed to attach overnight, followed by treatment with compounds **VP-16**, **10b**, **10g** and **10i** at indicated concentrations for 24 h. After 24 h media was discarded and cells were washed twice with PBS. Gently trypsinize and resuspend the cells in 1x binding buffer at a concentration of $1x10^6$ cells/mL. Incubate the cell suspension with 5 µL Annexin-V- FITC and 10 µL of propidium iodide for 10 min at room temperature and protect from light. Analysis was carried out by flow cytometry (FACSVerse, Becton-Dickinson, USA).

4.5. Molecular docking

The molecular docking studies were performed at the EVP binding site of the Topoisomerase –IIα (PDB ID: 5GWK) [47]. The co-ordinates of the crystal structure were obtained from RCSB-Protein Data Bank and suitable corrections to it were made by using Protein Preparation Wizard from Schrödinger package. In regard to the ligands, molecules were constructed using ChemBio3D Ultra 12.0 and their geometries were optimized using molecular mechanics. Finally, docking studies were performed on the most active conjugates (**10b, 10g** and **10i**) by using AutoDock 4.2 docking software [48] and the results were visualized through PyMOL [49].Conjugate **10b, 10g** and **10i** were shown in stick and

coloured by the atom type. Carbon: Cyan (**10b**), yellow (**10g**), Pink (**10i**), salmon (EVP); Oxygen: Red; Hydrogen: White; Nitrogen: Blue; Chlorine: Green; Fluorine: Ice blue.

References

1. C.P. Belani, L.A. Doyle, J. Aisner, Etoposide: Current status and future perspectives in the management of malignant neoplasms, Cancer Chemother. Pharmacol. 34 (1994) S118-126.
2. G. Kibria, H. Hatakeyama, H. Harashima, Cancer multidrug resistance: mechanisms involved and strategies for circumvention using a drug delivery system, Arch. Pharm. Res. 37 (2014) 4-15.
3. F.E. Koehn, G.T. Carter, The evolving role of natural products in drug discovery, Nat. Rev. Drug Discovery 4 (2005) 206-220.
4. D.J. Newman, G.M. Cragg, Microbial antitumor drugs: natural products of microbial origin as anticancer agents, Curr. Opin. Invest. Drugs 10 (2009) 1280-1296.
5. K.-H. Lee, Current Developments in the Discovery and Design of New Drug Candidates from Plant Natural Product Leads, J. Nat. Prod. 67 (2004) 273-283.
6. (a) H. Stahelin, Eur. J. Cancer 9 (1973) 215-221; (b) Z. Zhang, Z. Liu, L. Ma, S. Jiang, Y. Wang, H. Yu, Q. Yin, J. Cui, Y. Li, Mol. Pharmaceutics 10 (2013) 2426-2434; (c) A. Mariani, A. Bartoli, M. Atwal, K.C. Lee, C.A. Austin, R. Rodriguez, J. Med. Chem. 58 (2015) 4851-4856; (d) H. Stahelin, Eur. J. Cancer 6 (1970) 303-311.
7. K.R. Hande, Etoposide: Four decades of development of a topoisomerase II inhibitor, Eur. J. Cancer 34 (1998) 1514-1521.
8. E.L. Baldwin, N. Osheroff, Etoposide, topoisomerase II and cancer, Curr. Med. Chem.: Anti-Cancer Agents 5 (2005) 363-372.
9. (a) B.H. Long, L. Wang, A. Lorico, R.C. Wang, M.G. Brattain, A.M. Casazza, Cancer Res. 51 (1991) 5275-5283. (b) H. Helmbach, M.A. Kern, E. Rossmann, K. Renz, C. Kissel, B. Gschwendt, D. Schadendorf, J Invest Dermatol. 118 (2002) 923-932. (c) A. Alpsoy, S. Yasa, U. Gündüz, Biomed Pharmacother. 68 (2014) 351-355.
10. G.M. Keating, Rituximab: a review of its use in chronic lymphocytic leukaemia, low-grade or follicular lymphoma and diffuse large B-cell lymphoma, Drugs 70 (2010) 1445-1476.

11. W.A. Denny, B.C. Baguley, Dual topoisomerase I/II inhibitors in cancer therapy, Curr. Top. Med. Chem. 3 (2003) 339-353.

12. J.V. Walker, J.L. Nitiss, DNA topoisomerase II as a target for cancer chemotherapy, Cancer Invest. 20 (2002) 570-589.

13. J.L. Nitiss, Y.X. Liu, P. Harbury, M. Jannatipour, R. Wasserman, J. C. Wang, Amsacrine and etoposide hypersensitivity of yeast cells overexpressing DNA topoisomerase II, Cancer Res. 52 (1992) 4467-4472.

14. W.-H Cheng, B. Cao, H. Shang, C. Niu, L.-M. Zhang, Z.-H. Zhang, D.-L. Tian, S. Zhang, H. Chen, Z.-M. Zou, Synthesis and evaluation of novel podophyllotoxin derivatives as potential antitumor agents, Eur. J. Med. Chem. 85 (2014) 498-507.

15. M.K. Zilla, D. Nayak, R.A. Vishwakarma, P.R. Sharma, A. Goswami, A. Ali, A convergent synthesis of alkyneeazide cycloaddition derivatives of 4-a,b-2-propyne podophyllotoxin depicting potent cytotoxic activity, Eur. J. Med. Chem. 77 (2014) 47-55.

16. N. Shankaraiah, N.P. Kumar, S.B. Amula, S. Nekkanti, M.K. Jeengar, V.G.M. Naidu, T.S. Reddy, A. Kamal, One-pot synthesis of podophyllotoxin–thiourea congeners by employing NH_2SO_3H/NaI: Anticancer activity, DNA topoisomerase-II inhibition, and apoptosis inducing agents, Bioorg. Med. Chem. Lett. 25 (2015) 4239-4244.

17. C.Y. Sang, J.F. Liu, W.W. Qin, J. Zhao, L. Hui, Y.X. Jin, S.W. Chen, Synthesis and evaluation of the apoptosis inducing and CT DNA interaction properties of a series of 4β-carbamoyl 4′-O-demethylepipodophyllotoxins, Eur. J. Med. Chem. 70 (2013) 59-67.

18. J. M. Cassady, J. Doures, In Anti-Cancer Agents Based on Natural Products Models, Academic press, New York, 1980, p 319.

19. (a) B.F. Issell, Cancer Chemother. Pharmacol. 7 (1982) 73-80; (b) D. R. Budman, Semin. Oncol. 23 (1996) 8-14; (c) F.A. Greco, J.D. Hainsworth, Semin. Oncol. 23 (1996) 45-50.

20. A. Kamal, S.M. Ali Hussaini, M.S. Malik, Recent Developments Towards Podophyllotoxin Congeners as Potential Apoptosis Inducers, Anti-Cancer Agents in Medicinal Chemistry 15 (2015) 565-574.

21. I.V. Magedov, M. Manpadi, S.V. Slambrouck, W.F.A. Steelant, E. Rozhkova, N.M. Przheval'skii, S. Rogelj, A. Kornienko, Discovery and Investigation of Antiproliferative and Apoptosis-Inducing Properties of New Heterocyclic Podophyllotoxin Analogues Accessible by a One-Step Multicomponent Synthesis, J. Med. Chem. 50 (2007) 5183-5192.

22. A. Wieczorek, A. Błauż, A. Makal, B. Rychlik, D. Plażuk, Synthesis and evaluation of biological properties of ferrocenyl–podophyllotoxin conjugates, Dalton Trans. 46 (2017) 10847-10858.

23. L. Zhang, Z. Zhang, J. Wang, Y. Chen, F. Chen, Y. Lin, X. Zhu, Potential anti-MDR agents based on the podophyllotoxin scaffold: synthesis and antiproliferative activity evaluation against chronic myeloid leukemia cells by activating MAPK signaling pathways, RSC Adv. 6 (2016) 2895-2903.

24. T.S. Reddy, H. Kulhari, V.G. Reddy, A.V. Subba Rao,V. Bansal, A. Kamal, R. Shukla, Synthesis and biological evaluation of pyrazolo–triazole hybrids as cytotoxic and apoptosis inducing agents, Org. Biomol. Chem. 13 (2015) 10136-10149.

25. J.A. Stefely, R. Palchaudhuri, P.A. Miller, R.J. Peterson, G.C. Moraski, P.J. Hergenrother, M.J. Miller, N-((1-Benzyl-1H-1,2,3-triazol-4-yl)methyl)arylamide as a New Scaffold that Provides Rapid Access to Antimicrotubule Agents: Synthesis and Evaluation of Antiproliferative Activity Against Select Cancer Cell Lines, J. Med. Chem. 53 (2010) 3389-3395.

26. E. Bonandi, M.S. Christodoulou, G. Fumagalli, D. Perdicchia, G. Rastelli, D. Passarella, The 1,2,3-triazole ring as a bioisostere in medicinal chemistry, Drug Discov. Today 17 (2017) 1572-1581.

27. (a) A. Kamal, T.S. Reddy, S. Polepalli, S. Paidakula, V. Srinivasulu, V.G. Reddy, N. Jain, N. Shankaraiah, Bioorg. Med. Chem. Lett. 24 (2014) 3356-3360; (b) A. Kamal, P. Suresh, M.J. Ramaiah, T.S. Reddy, R.K. Kapavarapu, B.N. Rao, S. Imthiajali, T.L. Reddy, S.N.C.V.L. Pushpavalli, N. Shankaraiah, M. Pal-Bhadra, Bioorg. Med. Chem. 21 (2013) 5198-5208; (c) A. Kamal, T.S. Reddy, S. Polepalli, N. Shalini, V.G. Reddy, A.V. Subba Rao, N. Jain, N. Shankaraiah, Bioorg. Med. Chem. 22 (2014) 5466-5475.

28. Z.-J. Zhang, J. Tian, L.-T. Wang, M.-J. Wang, X. Nan, L. Yang, Y.-Q. Liu, S.L. Morris-Natschke, K.-H. Lee, Design, synthesis and cytotoxic activity of novel sulfonylurea derivatives of podophyllotoxin, Bioorg. Med. Chem. 22 (2014) 204-210.

29. T. Mosmann, Rapid colorimetric assay for cellular growth and survival: Application to proliferation and cytotoxicity assays, J. Immunol. Meth. 65 (1983) 55-63.

30. K S. Schwarz, B. Siewert, R. Csuk, A.P. Rauter, New antitumor 6-chloropurine nucleosides inducing apoptosis and G2/M cell cycle arrest, Euro. J. Med. Chem. 90 (2015) 595-602.

31. H.J. Park, H.-J. Lee, E.-J. Lee, H.J. Hwang, S.-H. Shin, M.-E. Suh, C.Kim, H.J. Kim, E.-K. Seo, S.K. Lee, Cytotoxicity and DNA Topoisomerase Inhibitory Activity of Benz[f]indole-4,9-dione Analogs, Biosci. Biotechnol. Biochem. 67 (2003) 1944-1949.

32. S. Bansal, D. Sinha,M. Singh, B. Cheng,Y.-C. Tse-Dinh, V. Tandon, 3,4-Dimethoxyphenyl bis-benzimidazole, a novel DNA topoisomerase inhibitor that preferentially targets Escherichia coli topoisomerase I, J. Antimicrob. Chemother. 67 (2012) 2882-2891.

33. M. Yao, J. Yang, L. Cao, L. Zhang, S. Qu, H. Gao, Saikosaponin-d inhibits proliferation of DU145 human prostate cancer cells by inducing apoptosis and arresting the cell cycle at G0/G1 phase, Mol. Med. Rep. 10 (2014) 365-372.

34. S. Allen, J. Sotos, M.J. Sylte, C.J. Czuprynski, Use of Hoechst 33342 staining to detect apoptotic changes in bovine mononuclear phagocytes infected with Mycobacterium avium subsp. paratuberculosis, Clin. Diagn. Lab Immunol. 8 (2001) 460-464.

35. J.D. Ly, D.R. Grubb, A. Lawen, The mitochondrial membrane potential (Δψm) in apoptosis; an update, Apoptosis 8 (2003) 115-128.

36. A. Parvin, R. Pranap, U. Shalini, A. Devendran, J.E. Baker, A. Dhanasekaran, Erythropoietin protects cardiomyocytes from cell death during hypoxia/reperfusion injury through activation of survival signaling pathways, PloS one 9 (2014), e107453.

37. L.G. Rodriguez, X. Wu, J. L. Guan, Wound healing assay, Methods Mol. Biol. 294 (2005) 23-29.

38. H.Y. Kim, J.H. Ryu, C.W. Chu, G.M. Son, Y.I. Jeong, T.W. Kwak, D.H. Kim, C.W. Chung, Y.H. Rhee, D.H. Kang, H.M. Kim, Paclitaxel-incorporated nanoparticles using block copolymers composed of poly (ethylene glycol)/poly (3-hydroxyoctanoate), Nanoscale Res. Lett. 9 (2014) 525-534.

39. (a) A. Kamal, B. Shaik, V.L. Nayak, B. Nagaraju, J.S. Kapure, M.S. Malik, T.B. Shaik, B. Prasad, Bioorg. Med. Chem. 22 (2014) 5155–5167. (b) J. Zhao, H. Zhao, J.A. Hall, D. Brown, E. Brandes, J. Bazzill, P.T. Grogan, C. Subramanian, G. Vielhauer, M.S. Cohen, B.S.J. Blagg, Med. Chem. Commun. 5 (2014) 1317-1323.

40. (a) A. Berenyi, A. Minorics, R. Ivanyi, et al. Steroids 78 (2013) 69–78; (b) B. Das, C.R. Reddy, J. Kashanna, S.M. Mamidyala, C.G. Kumar, Med. Chem. Res. 21 (2012) 3321–3325; (c) T.J. Mosmann, Immunol. Meth. 65 (1983) 55-63.

41. M. Rosner, K. Schipany, M. Hengstschläger, Merging high-quality biochemical fractionation with a refined flow cytometry approach to monitor nucleocytoplasmic protein expression throughout the unperturbed mammalian cell cycle, Nature Protocols 8 (2013) 602-626.

42. P. Moongkarndi, N. Kosem, S. Kaslungka, O. Luanratana, N. Pongpan, N. Neungton, Antiproliferation, antioxidation and induction of apoptosis by Garcinia mangostana (mangosteen) on SKBR3 human breast cancer cell line, J. Ethnopharmacol. 90 (2004) 161-166.

43. A. Pataer, M.A. Fanale, J.A. Roth, S.G. Swisher, K.K. Hunt, Induction of apoptosis in human lung cancer cells following treatment with amifostine and an adenoviral vector containing wild-type p53, Cancer gene therapy 13 (2006) 806-814.

44. M. Reers, S.T. Smiley, C. Mottola-Hartshorn, A. Chen, M. Lin, L.B. Chen, Mitochondrial membrane potential monitored by JC-1 dye, Methods in enzymology 260 (1995) 406-417.

45. C.C. Liang, A.Y. Park, J.-L. Guan, In vitro scratch assay: a convenient and inexpensive method for analysis of cell migration in vitro, Nature Protocols 2 (2007) 329-333.

46. S. Deng, Y. Yang, Y. Han, X. Li, X. Wang, X. Li, Z. Zhang, Y. Wang, UCP2 inhibits ROS-mediated apoptosis in A549 under hypoxic conditions, PloS One 7 (2012) e30714.

47. Y.R. Wang, S.F. Chen, C.C. Wu, Y.W. Liao, T.S Lin, K.T. Liu, Y.S. Chen, T.K. Li, T.C. Chien, N.L. Chan, Producing irreversible topoisomerase II-mediated DNA breaks bysite-specific Pt(II)-methionine coordination chemistry, Nucleic Acids Res.45 (2017) 10861-10871.

48. G.M. Morris, R. Huey, W. Lindstrom, M.F. Sanner, R.K. Belew, D.S. Goodsell, A.J. Olson, AutoDock4 and AutoDockTools4: Automated docking with selective receptor flexibility, J. Comput. Chem. 30 (2009) 2785-2791.
49. W.L. Delano, The PyMOL Molecular Graphics System, DeLano Scientific: San Carlos, CA, USA, 2002.

Figure/Scheme Captions

Scheme 1. General Synthesis of substituted aryl/benzyl triazolic acid derivatives (**6a-i** and **7a-k**). Reagents and conditions: (i) different substituted aryl/benzyl azides, $CuSO_4.5H_2O$, sodium ascorbate, *t*-BuOH/H_2O (1:1), rt, 12 h; (ii) LiOH, THF:H_2O (1:1), rt, overnight.

Scheme 2. General synthesis of 4*β*-amidotriazole linked podophyllotoxin derivatives (**10a-i** and **11a-k**). Reagents and conditions: (i) NaN_3, CF_3COOH, DCM, 0 °C-rt, 4 h; (ii) H_2, Pd/C, EtOAc, 8 h, rt; (iii) anhydrous.DMF, EDCI, HOBT, 0 °C-rt, 12h.

Table 1. $^{a}IC_{50}$ values (in µM) for compounds (**10a-i** and **11a-k**) in selected human cancer cell lines.

Fig. 1. Structure of podophyllotoxin and its semi-synthetic derivatives.

Fig. 2. Flow cytometric analysis: **a**) DU-145 cells were treated with compounds **VP-16**, **10b**, **10g,** and **10i** at indicated concentrations for 24 h. **b**) Percentage of DNA content in the treated groups was presented in the bar graph.

Fig. 3. Effect of the synthesized compounds **10b**, **10g,** and **10i** on topo II. Lane A: Linear DNA; Lane B: Decatenated DNA; Lane C: Catenated DNA; Lane D: Catenated DNA + topo II; Lane E: Catenated DNA + topo II (5 units) + Etoposide (100 µM); Lane F: Catenated DNA + topo II + Compound **10b** (100 µM); Lane G: Catenated DNA + topo II + Compound **10g** (100 µM); Lane H: Catenated DNA + topo II + Compound **10i** (100 µM).

Fig. 4. Morphological changes of DU-145 cells. Effect of compounds **10b**, **10g,** and **10i** on morphological features and cell viability of DU-145 cells.

Fig. 5. Hoechst staining for apoptosis. Condensation and fragmentation of chromatin was observed in DU-145 cells treated with compounds **VP-16**, **10b**, **10g,** and **10i**. Randomly

selected various fields in each treatment were counted for chromatin condensation and nuclear fragmentation.

Fig. 6. Compounds induce mitochondrial membrane potential in DU-145 cells. **a**) Cells were treated with compounds **VP-16**, **10b**, **10g,** and **10i** for 24 h and observed changes in mitochondrial membrane potential by flow cytometry. **b**) Bar graph represents the percentage distribution of J-aggregates and J-monomer cells in all groups.

Fig. 7. Determination of ROS generation in DU-145. **a)** Fluorescence images are obtained from the cells treated with the compounds **VP-16**, **10b**, **10g,** and **10i** for 24 h and then observed the production of ROS by DCFDA. **b)** Bar graph represents the mean fluorescence intensity.

Fig. 8. *In vitro* scratch assay on DU-145 cells. Phase contrast images were obtained by the treatment of compounds **VP-16**, **10b**, **10g,** and **10i** at indicated concentrations for 0, 24 and 48 h.

Fig. 9. Compounds induce apoptosis in DU-145 cells. **a)** Cells were treated with compounds **VP-16**, **10b**, **10g,** and **10i** for 24 h. Cells were labeled with Annexin V FITC, PI and analyzed in flow cytometry. **b)** Percentage of cells in the each phase was represented in the bar graph.

Fig. 10. A) Surface binding pose of conjugate **10b, 10g,** and **10i** in EVP binding pocket **B)** Binding pose comparison of conjugate **10g** with EVP at intercalation site of DNA topoisomerases-IIα. Conjugate **10b, 10g,** and **10i** were shown in stick and colored by the atom type. Carbon: Cyan (**10b**), yellow (**10g**), Pink (**10i**), salmon (EVP); Oxygen: Red; Hydrogen: White; Nitrogen: Blue; Chlorine: Green; Fluorine: Ice blue.

Fig. 11. A) B) and **C)** Hydrogen bonding of conjugate **10b, 10g,** and **10i** respectively in EVP binding pocket of topoisomerases-IIα.

Fig. 12. A), B) and **C)** Binding pose of conjugate **10b, 10g,** and **10i** respectively, including hydrophobic interactions in EVP binding pocket of tubulin (PDB ID: 5GWK).

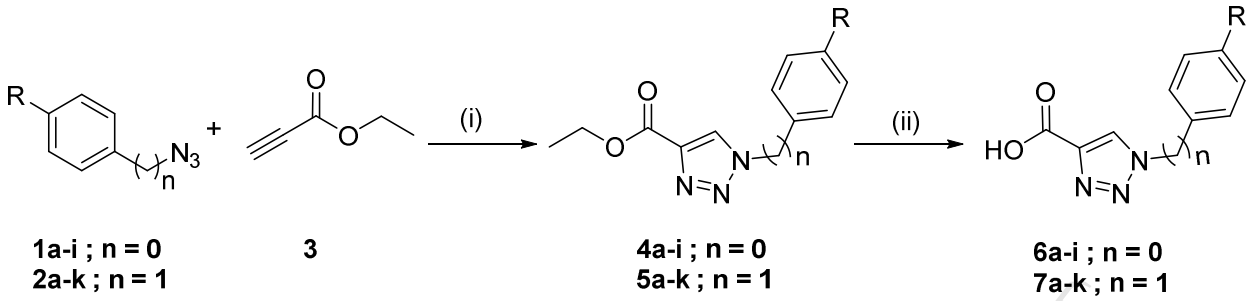

Scheme 1. General Synthesis of substituted aryl/benzyl triazolic acid derivatives (**6a-i** and **7a-k**). Reagents and conditions: (i) different substituted aryl/benzyl azides, $CuSO_4.5H_2O$, sodium ascorbate, *t*-BuOH/H_2O (1:1), rt, 12 h; (ii) LiOH, THF:H_2O (1:1), rt, overnight.

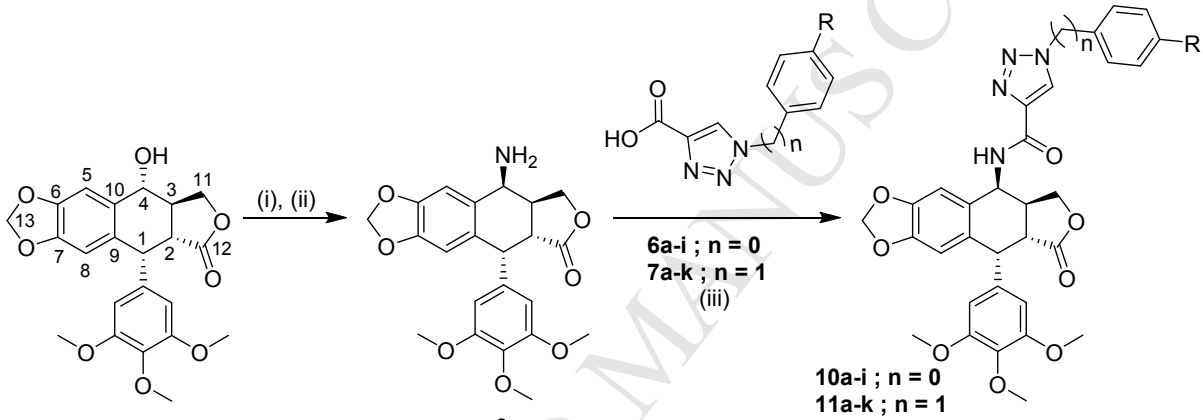

n = 0	n = 1
10a; R = H	11a; R = H
10b; R = 4-OMe	11b; R = 4-OMe
10c; R = 3,4-OMe	11c; R = 3-OMe
10d; R = 3,5-OMe	11d; R = 3,4-OMe
10e; R = 3,4,5-OMe	11e; R = 3,5-OMe
10f; R = 3,4-Meth.dioxy	11f; R = 3,4,5-OMe
10g; R = Cl	11g; R = 3,4-Meth.dioxy
10h; R = F	11h; R = Cl
10i; R = CF_3	11i; R = F
	11j; R = CF_3
	11k; R = m-phenoxy

Scheme 2. General synthesis of 4*β*-amidotriazole linked podophyllotoxin derivatives (**10a-i** and **11a-k**). Reagents and conditions: (i) NaN_3, CF_3COOH, DCM, 0 °C-rt, 4 h; (ii) H_2, Pd/C, EtOAc, 8 h, rt; (iii) anhydrous.DMF, EDCI, HOBT, 0 °C-rt, 12h.

Table 1. [a]IC_{50} values (in µM) for compounds (**10a-i** and **11a-k**) in selected human cancer cell lines

Compound	Hela[b]	MCF-7[c]	DU-145[d]	A549[e]	HepG2[f]	HT-29[g]	NIH/3T3[h]
10a	2.47±0.24	1.45±0.46	1.31±0.11	1.82±0.11	1.94±0.13	5.37±0.74	53.86±1.26
10b	6.49±0.22	1.11±0.10	**0.99±0.07**	1.61±0.38	2.79±0.54	11.40±1.66	62.89±2.07
10c	18.55±2.22	8.036±0.58	14.50±2.74	12.15±0.04	11.67±0.37	15.11±1.40	66.23±1.99
10d	17.00±4.16	8.656±0.26	11.66±1.27	17.72±0.86	13.75±0.62	19.59±0.35	76.95±4.44
10e	10.21±0.66	7.338±0.13	8.545±0.69	14.68±1.25	0.957±0.026	8.545±0.69	79.62±1.42
10f	47.69±8.49	7.614±0.77	8.918±0.46	0.974±0.03	9.939±0.58	17.86±0.46	67.25±4.36
10g	0.78±0.02	0.97±0.12	**0.70±0.01**	1.20±0.01	0.78±0.08	4.11±0.71	89.04±0.73
10h	78.61±1.15	6.699±0.06	9.441±0.12	14.06±4.02	10.91±1.16	13.82±0.48	98.13±5.30
10i	1.21±0.27	1.35±0.07	**0.89±0.02**	1.96±0.08	1.21±0.27	4.40±0.05	83.82±3.35
11a	18.81±0.70	13.70±0.35	17.13±2.34	13.33±0.47	13.14±0.16	19.07±1.24	67.02±4.84
11b	3.46±0.06	3.32±0.55	1.76±0.27	5.82±0.43	1.96±0.07	17.53±0.34	66.97±3.40
11c	22.61±2.71	7.711±0.22	12.41±2.10	21.33±0.76	9.88±0.16	31.29±3.01	74.06±3.17
11d	12.40±0.46	12.19±0.19	13.53±0.15	19.64±3.38	12.66±0.89	13.53±1.78	83.75±4.51
11e	25.81±6.28	13.94±1.08	14.64±0.65	32.39±2.10	14.23±0.33	27.37±4.98	81.31±1.34
11f	10.21±0.66	7.338±0.13	8.545±0.69	14.68±1.25	0.957±0.026	8.545±0.69	61.95±0.69
11g	32.87±3.67	34.54±3.68	27.69±6.84	34.46±0.85	26.57±3.70	36.35±2.95	69.48±1.60
11h	3.57±0.16	5.30±0.39	2.37±0.08	8.06±0.06	3.54±0.37	23.71±0.38	81.26±1.03
11i	28.99±0.45	19.13±2.53	22.77v3.27	75.69±2.21	34.09±1.39	78.33±1.17	91.14±3.33
11j	26.62±4.28	21.92±1.94	32.94±1.87	27.84±1.43	20.38±1.77	66.42±3.67	75.50±2.24
11k	22.68±1.07	4.395±0.50	5.677±0.22	8.652±3.08	6.604±0.56	40.47±1.25	88.40±3.70
Etoposide	2.71±0.52	1.62±0.14	2.35±0.05	1.97±0.17	2.84±0.27	1.87±0.31	-
Podophyllotoxin	3.45±0.29	3.06±0.24	4.15±0.63	4.60±0.42	6.63±0.17	4.78±0.16	-

[a]50% Inhibitory concentration after 48 h of drug treatment and the values are an average of three individual experiments. [b]cervical, [c]breast, [d]prostate, [e]lung, [f]liver, [g]colon, and [h]normal fibroblast cells.

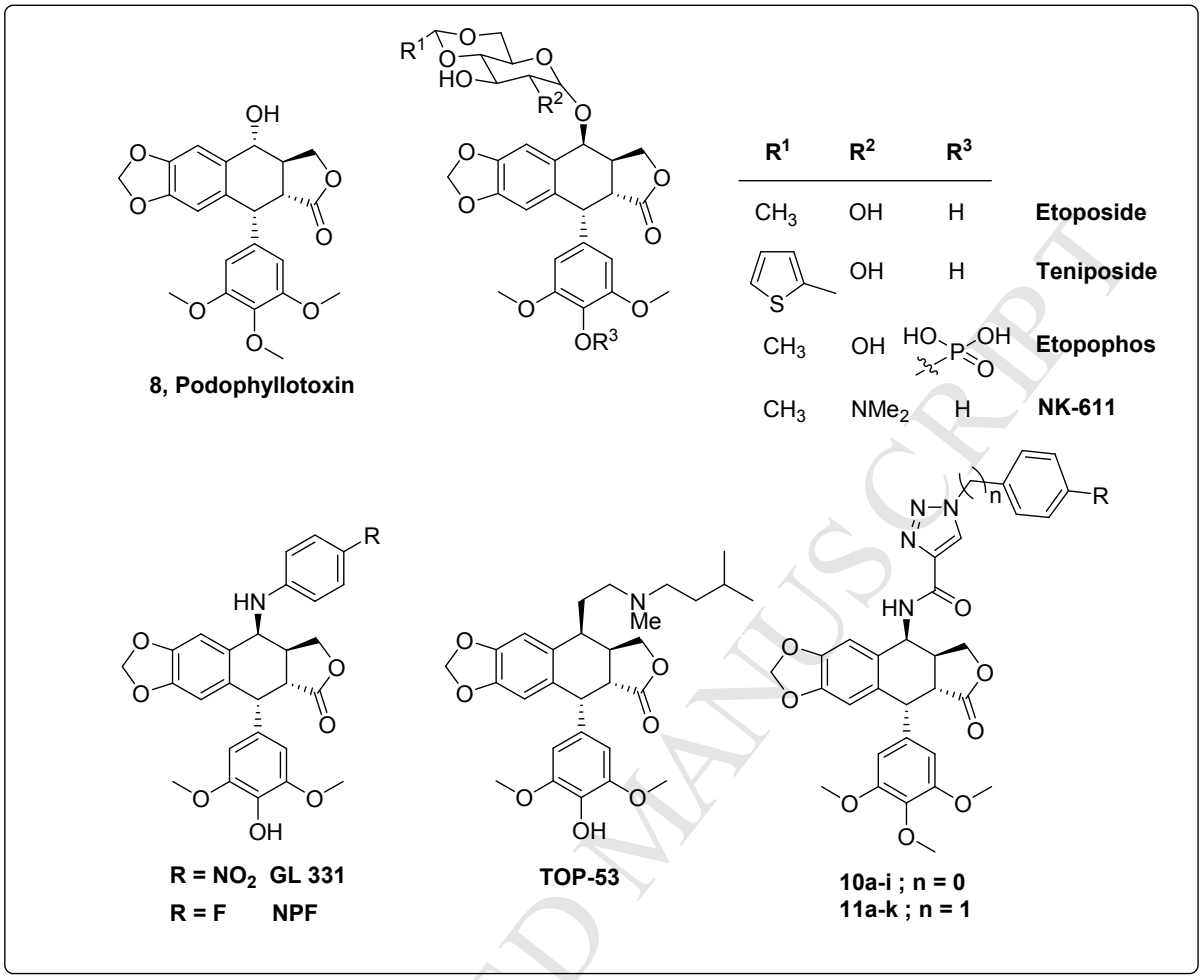

Fig. 1. Structure of podophyllotoxin and its semi-synthetic derivatives.

a)

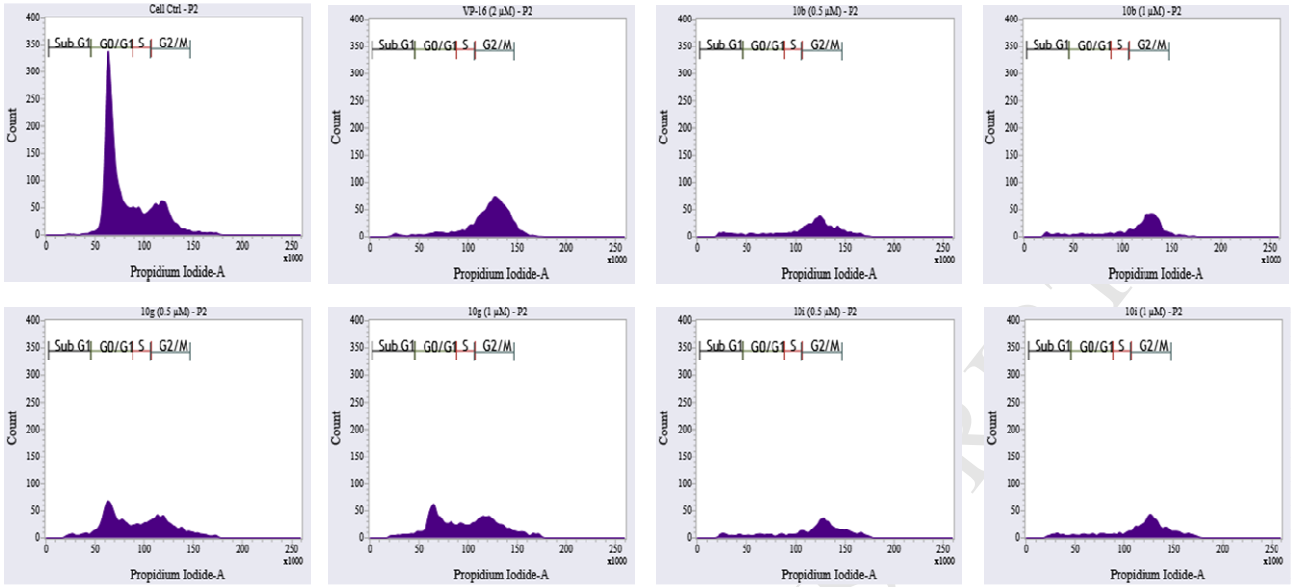

b)

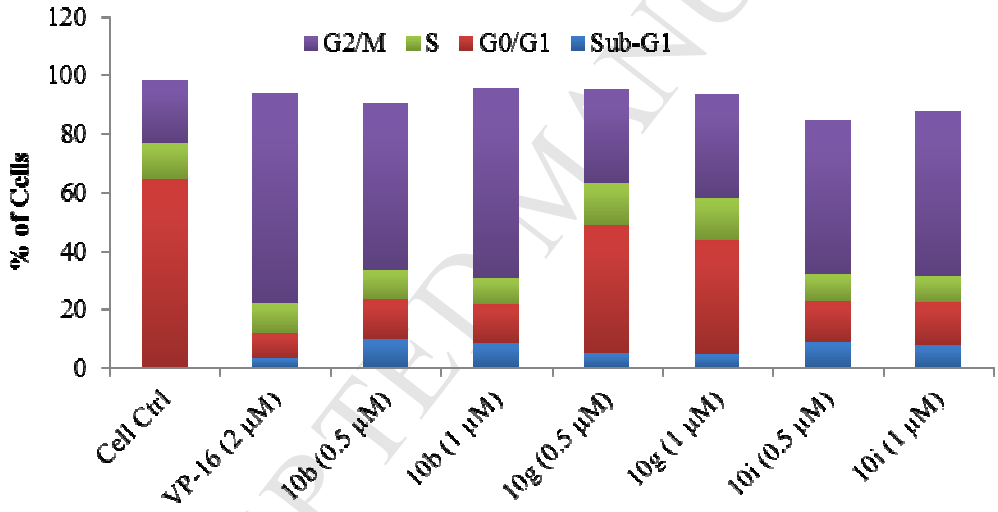

Fig. 2. Flow cytometric analysis: **a**) DU-145 cells were treated with compounds **VP-16**, **10b**, **10g,** and **10i** at indicated concentrations for 24 h. **b**) Percentage of DNA content in the treated groups was presented in the bar graph.

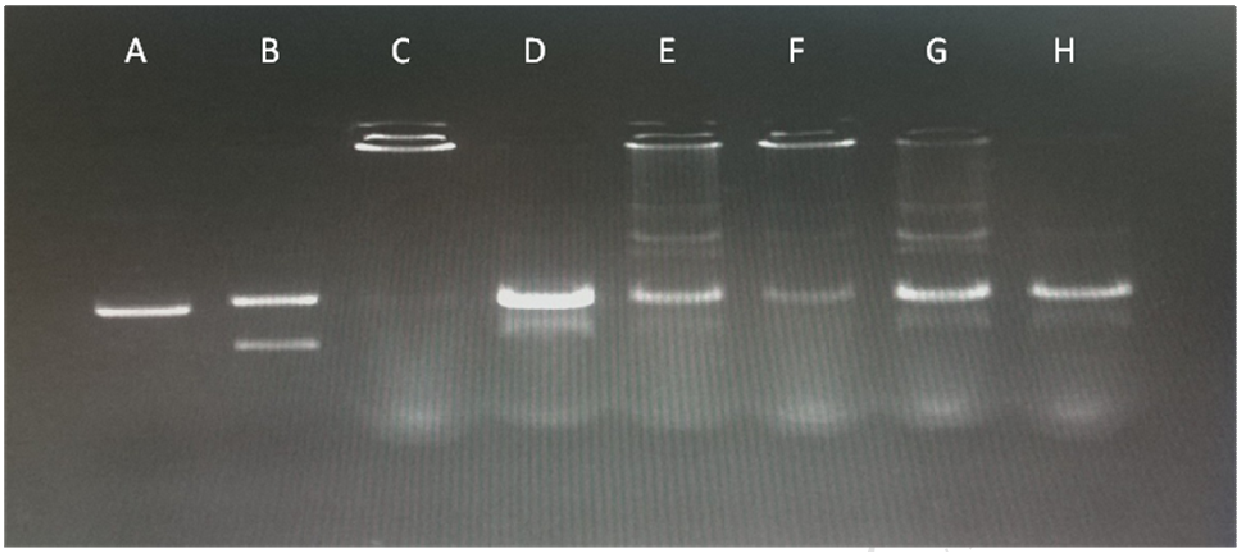

Fig. 3. Effect of the synthesized compounds **10b**, **10g,** and **10i** on topo II. Lane A: Linear DNA; Lane B: Decatenated DNA; Lane C: Catenated DNA; Lane D: Catenated DNA + topo II; Lane E: Catenated DNA + topo II (5 units) + Etoposide (100 µM); Lane F: Catenated DNA + topo II + Compound **10b** (100 µM); Lane G: Catenated DNA + topo II + Compound **10g** (100 µM); Lane H: Catenated DNA + topo II + Compound **10i** (100 µM).

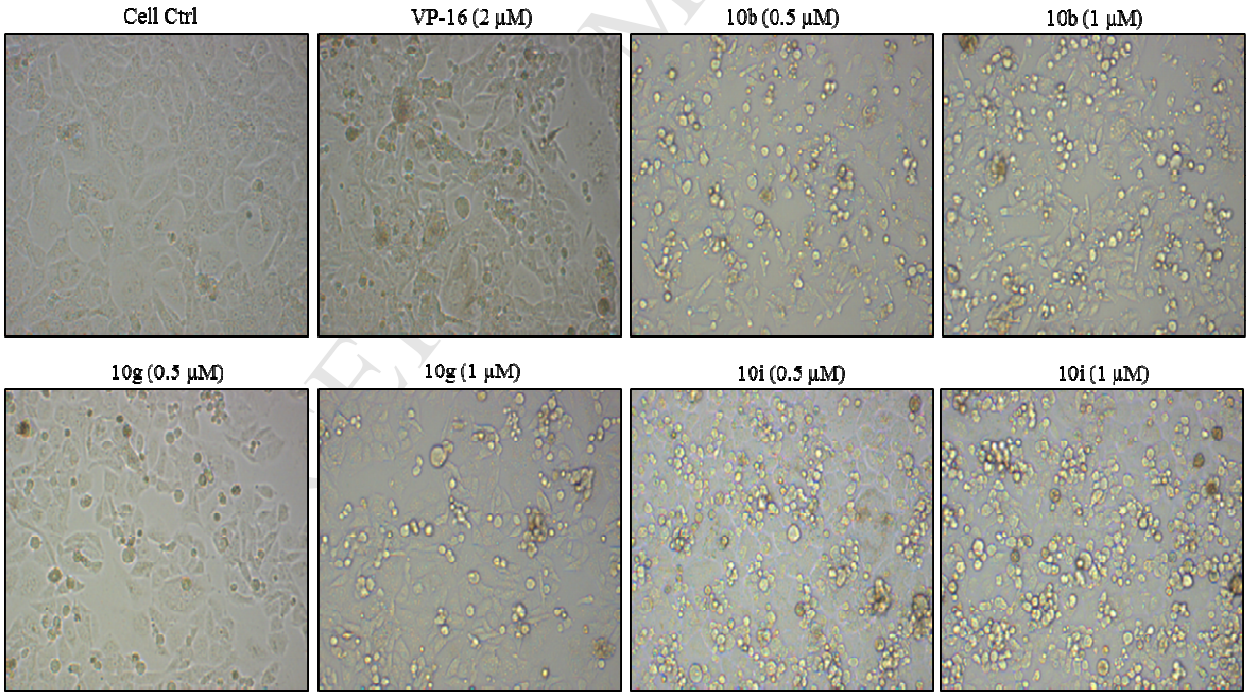

Fig. 4. Morphological changes of DU-145 cells. Effect of compounds **10b**, **10g,** and **10i** on morphological features and cell viability of DU-145 cells.

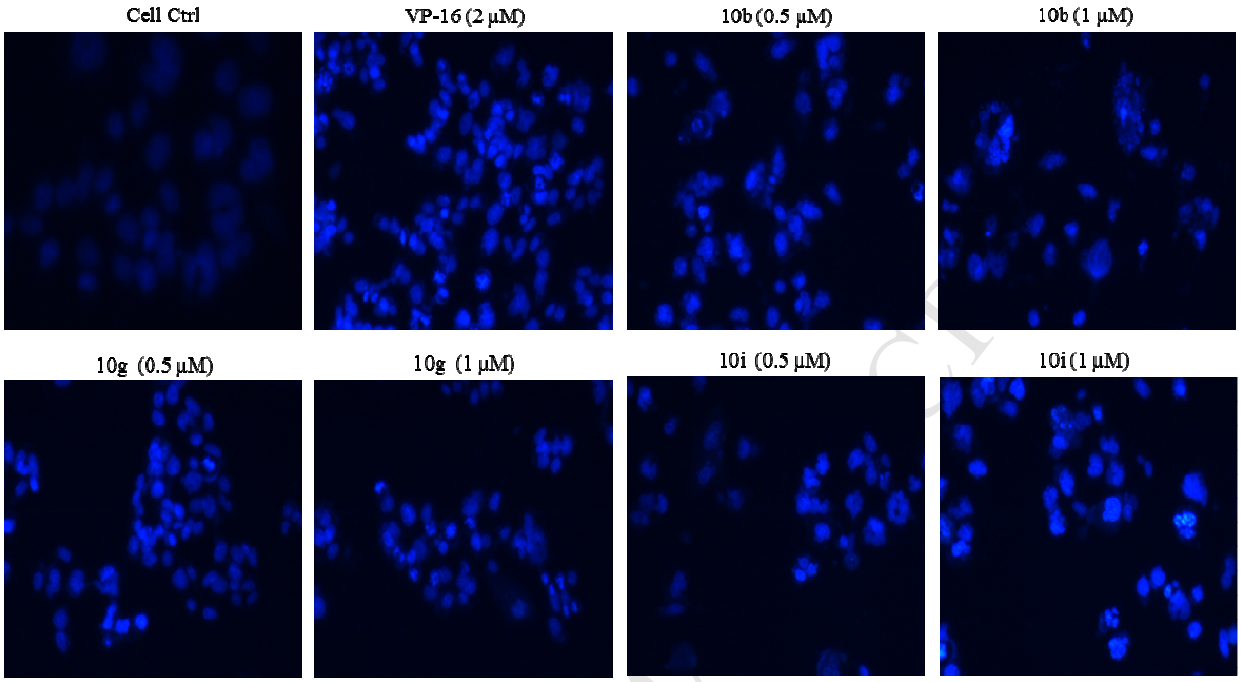

Fig. 5. Hoechst staining for apoptosis. Condensation and fragmentation of chromatin was observed in DU-145 cells treated with compounds **VP-16**, **10b**, **10g,** and **10i**. Randomly selected various fields in each treatment were counted for chromatin condensation and nuclear fragmentation.

a)

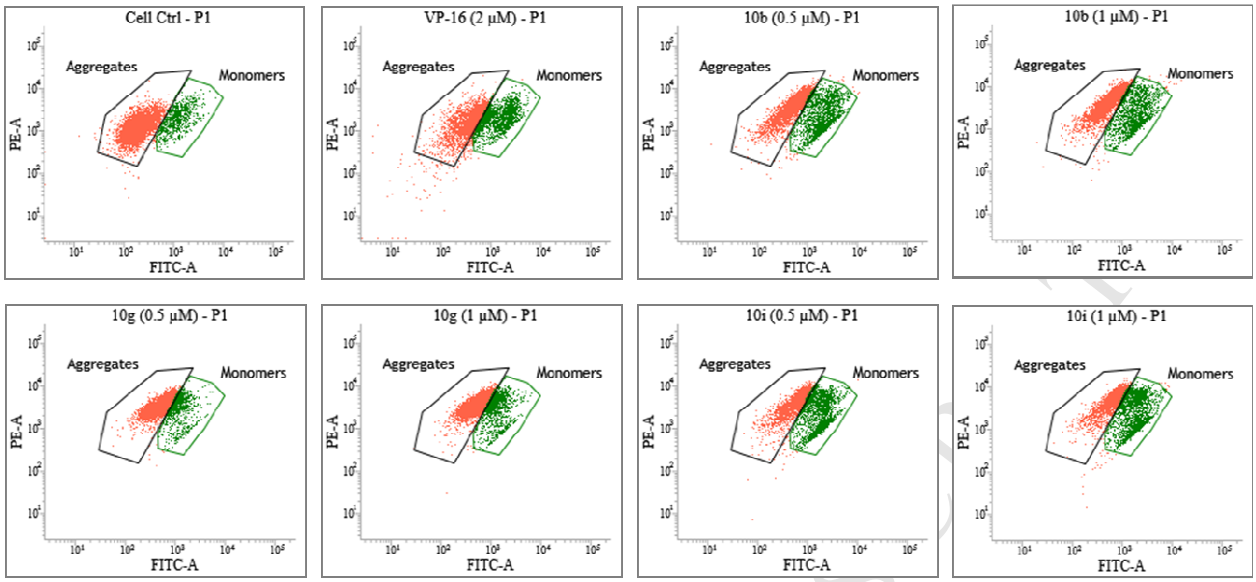

b)

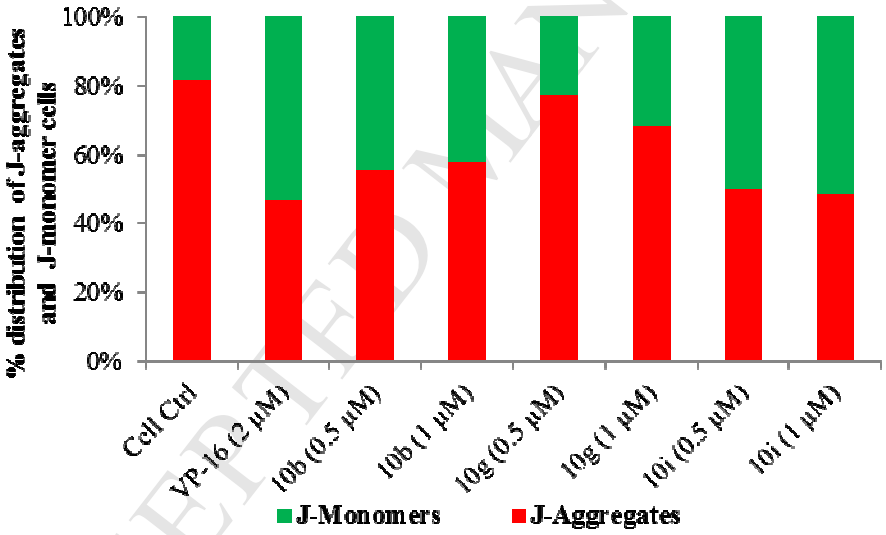

Fig. 6. Compounds induce mitochondrial membrane potential in DU-145 cells. **a**) Cells were treated with compounds **VP-16**, **10b**, **10g,** and **10i** for 24 h and observed changes in mitochondrial membrane potential by flow cytometry. **b**) Bar graph represents the percentage distribution of J-aggregates and J-monomer cells in all groups.

a)

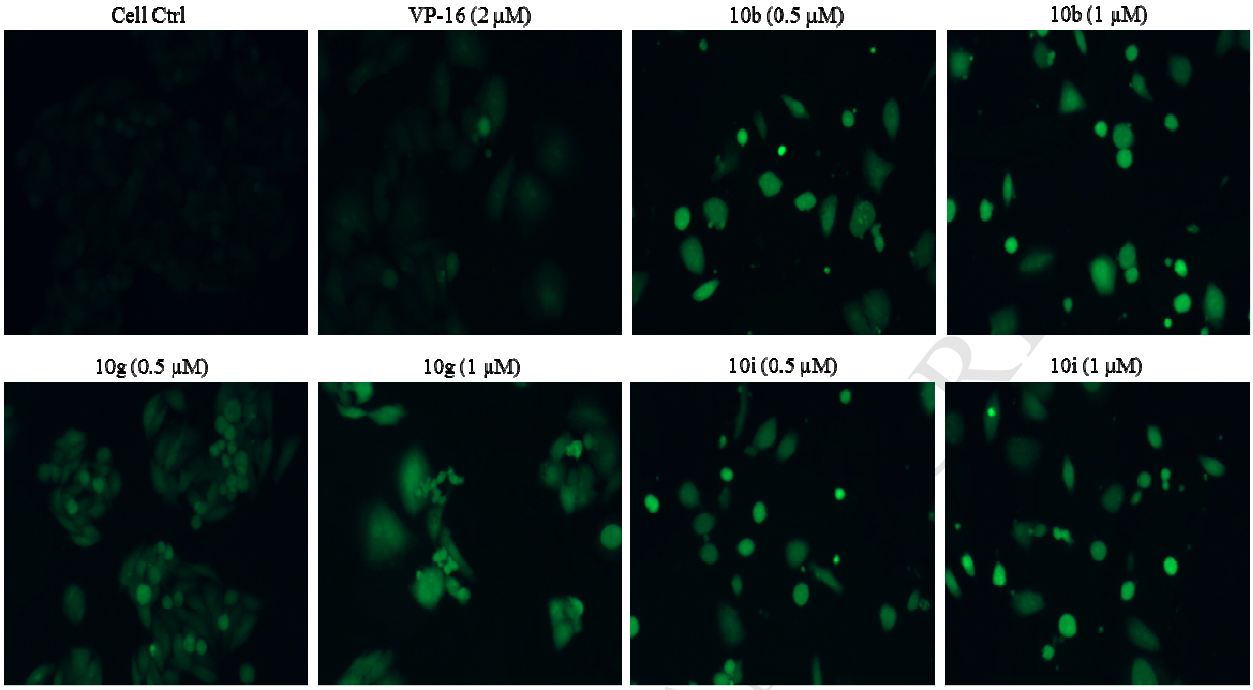

b)

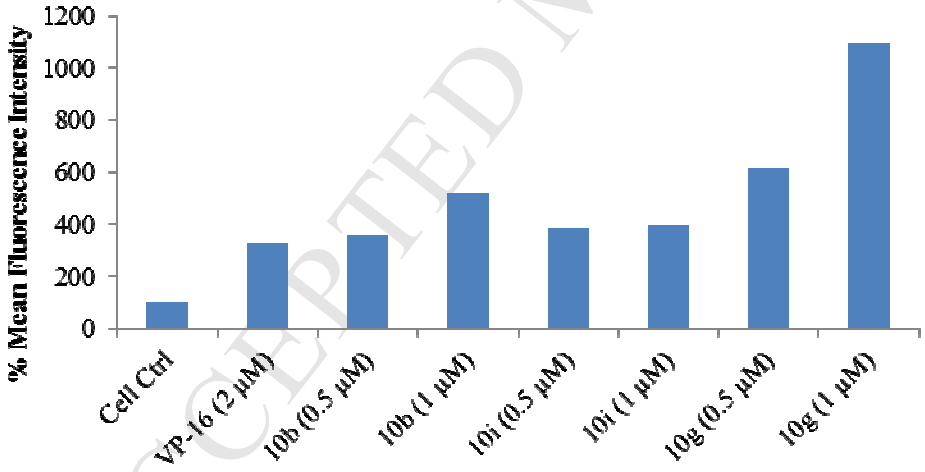

Fig. 7. Determination of ROS generation in DU-145. **a)** Fluorescence images are obtained from the cells treated with the compounds **VP-16**, **10b**, **10g,** and **10i** for 24 h and then observed the production of ROS by DCFDA. **b)** Bar graph represents the mean fluorescence intensity.

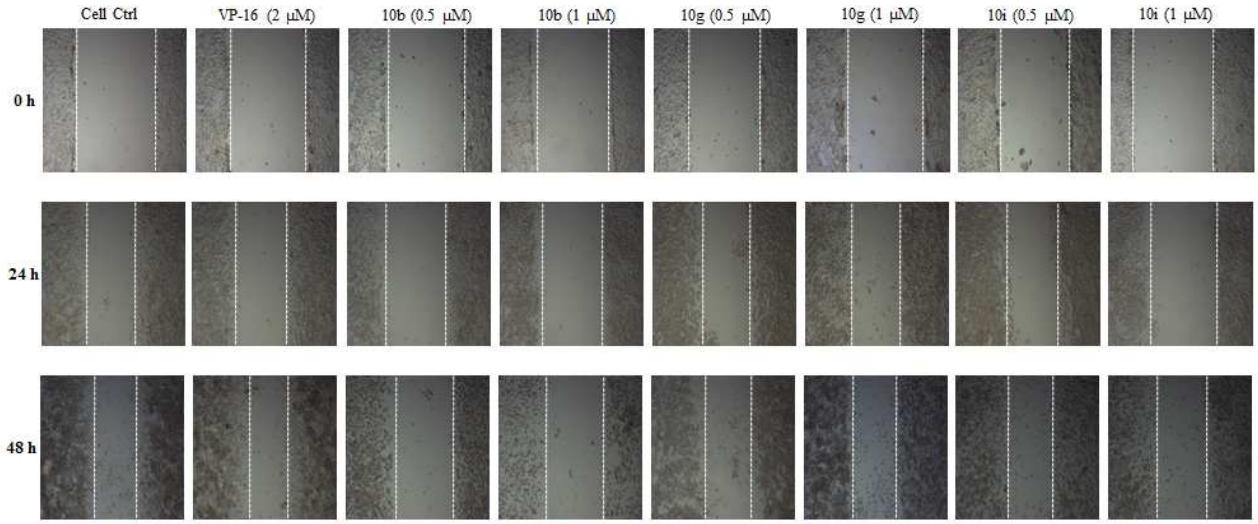

Fig. 8. *In vitro* scratch assay on DU-145 cells. Phase contrast images were obtained by the treatment of compounds **VP-16**, **10b**, **10g,** and **10i** at indicated concentrations for 0, 24 and 48 h.

a)

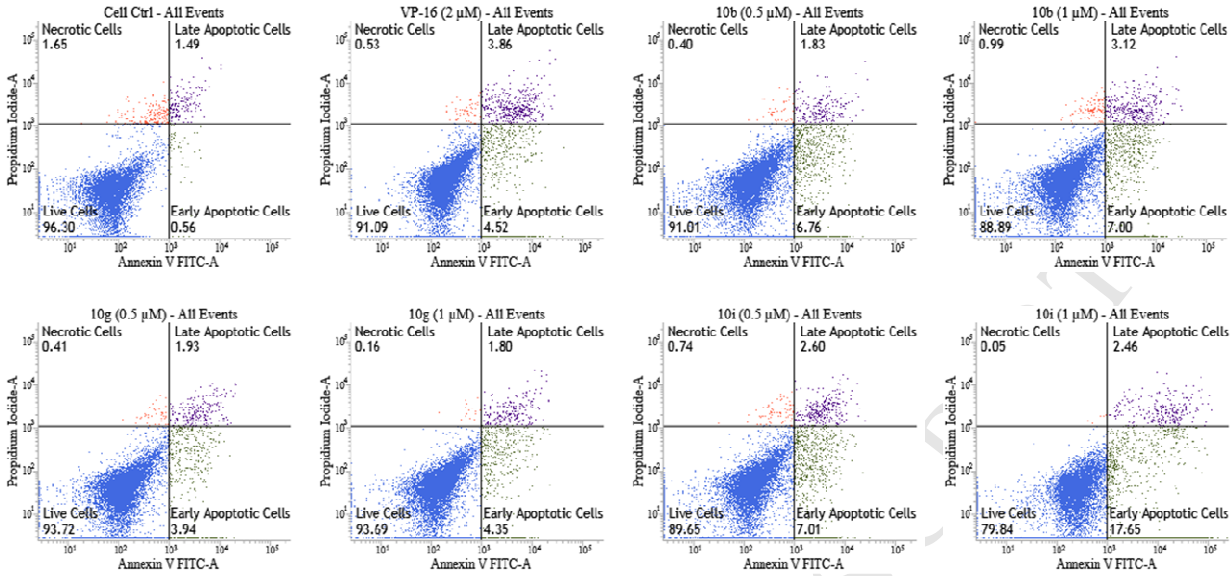

b)

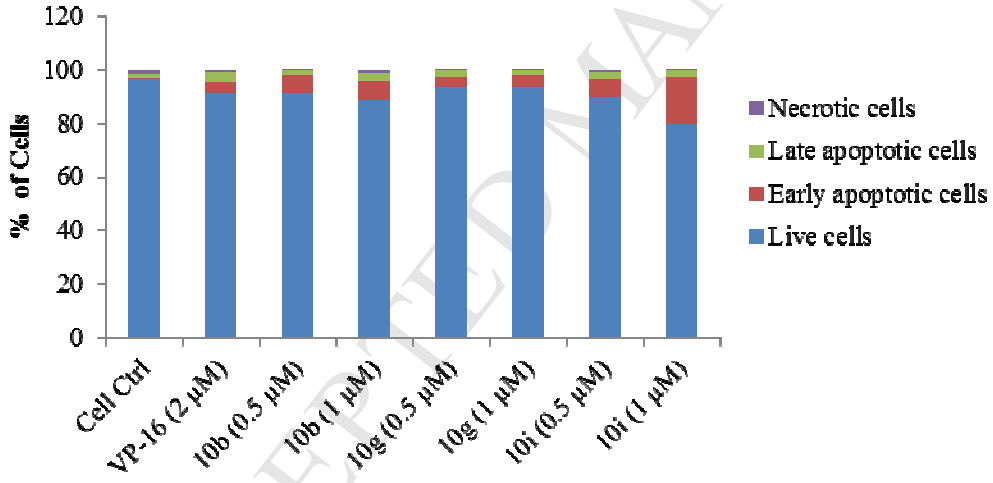

Fig. 9. Compounds induce apoptosis in DU-145 cells. **a)** Cells were treated with compounds **VP-16**, **10b**, **10g,** and **10i** for 24 h. Cells were labeled with Annexin V FITC, PI and analyzed in flow cytometry. **b)** Percentage of cells in the each phase was represented in the bar graph.

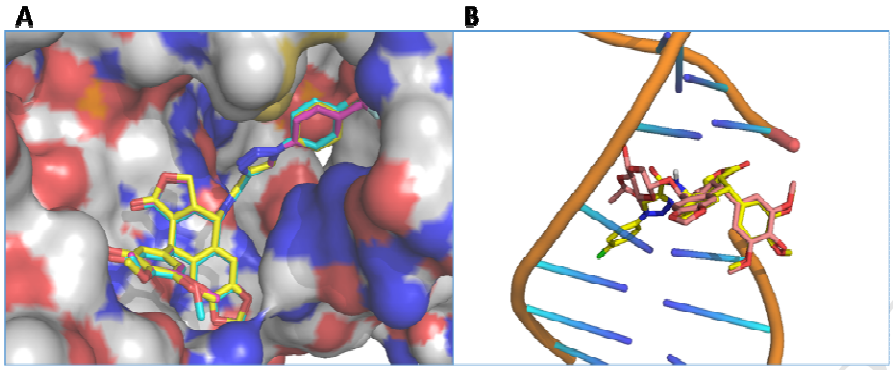

Fig. 10. A) Surface binding pose of conjugate **10b, 10g,** and **10i** in EVP binding pocket **B)** Binding pose comparison of conjugate **10g** with EVP at intercalation site of DNA topoisomerases-IIα. Conjugate **10b, 10g,** and **10i** were shown in stick and colored by the atom type. Carbon: Cyan (**10b**), yellow (**10g**), Pink (**10i**), salmon (EVP); Oxygen: Red; Hydrogen: White; Nitrogen: Blue; Chlorine: Green; Fluorine: Ice blue.

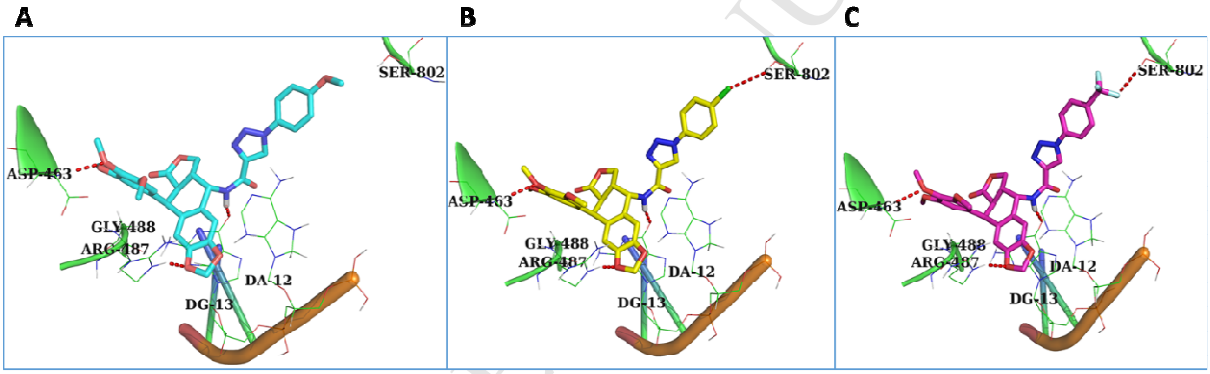

Fig. 11. A) B) and **C)** Hydrogen bonding of conjugate **10b, 10g,** and **10i** respectively in EVP binding pocket of topoisomerases-IIα.

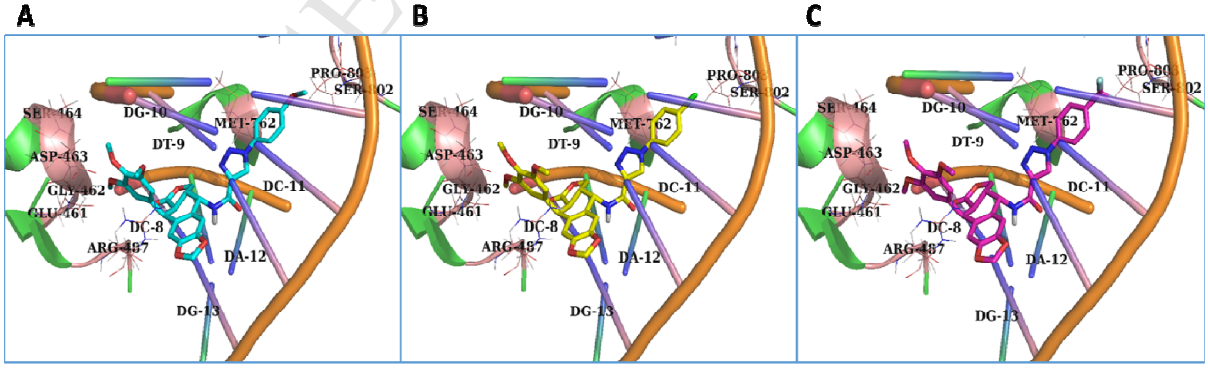

Fig. 12. A), B) and **C)** Binding pose of conjugate **10b, 10g,** and **10i** respectively, including hydrophobic interactions in EVP binding pocket of tubulin (PDB ID: 5GWK).

Research Highlights

1. In the present work **20** derivatives (**10a-i and 11a-k**) were synthesized and tested for their antiproliferative activity.
2. Compounds **10b, 10g** and **10i** showed significant cytotoxicity with IC_{50} values of, < 1 μM against the tested human cancer cell lines.
3. Compounds (**10b, 10g** and **10i**) induce cell cycle arrest in the G2/M phase.
4. Topoisomerase-mediated DNA relaxation assay results showed that the derivatives could effectively inhibit the activity of Topoisomerase-II.
5. The apoptotic studies were showed that this class of compounds could induce apoptosis of DU-145 cells.
6. Compounds (**10b, 10g** and **10i**) can be considered as interesting lead molecules for further development of more potent anticancer agents against prostate cancer cells.